I&EC research
Industrial & Engineering Chemistry Research

Article

Cite This: Ind. Eng. Chem. Res. 2019, 58, 17489−17506

pubs.acs.org/IECR

Novel Adsorption Process for Co-Production of Hydrogen and CO_2 from a Multicomponent Stream

Anne Streb,[†] Max Hefti,[†] Matteo Gazzani,*[,‡] and Marco Mazzotti*[,†]

[†]ETH Zurich, Institute of Process Engineering, Zurich 8092, Switzerland

[‡]Utrecht University, Copernicus Institute of Sustainable Development, 3512 JE Utrecht, The Netherlands

Supporting Information

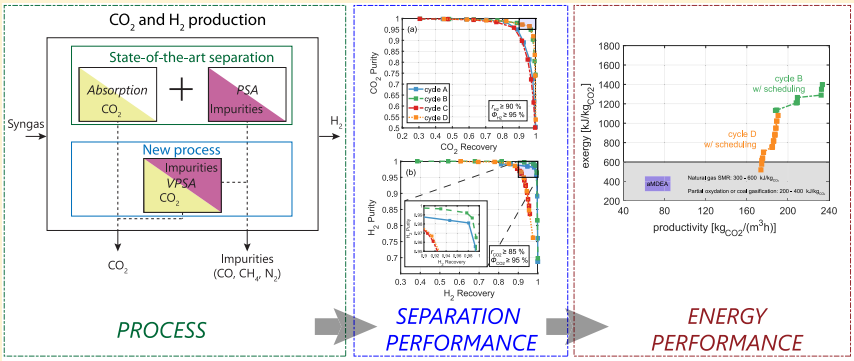

ABSTRACT: The production of carbon-neutral H_2 is pivotal for reaching net-zero CO_2 in 2050. Undoubtedly, the time and scale of this transition call for the decarbonization of H_2 production from natural gas, where the separation processes account for a large share of the capital and operational expenditures. Energy- and cost-efficient processes are therefore highly sought after. With this contribution, we have developed, modeled, and optimized new vacuum pressure swing adsorption (VPSA) cycles for co-production of high-purity, high-recovery CO_2 and H_2 from a ternary feed stream with a significant amount of an impurity. We identified two cycles that can purify CO_2 up to 95% with recoveries greater 90% while co-producing hydrogen with the same specifications. Key cycle features include purge under vacuum with part of the hydrogen product and recycle of the hydrogen-rich outflow during the initial part of the blowdown. The latter should be carried out via a compressor for very high hydrogen purities and recoveries, or via a sequence of pressure equalization (PE) steps for the targeted separation, which also drastically reduces the energy consumption. The volumetric productivity ranges from 160 to 240 $kg_{CO_2}/m^3/h$, which is significantly larger than the available open data for absorption-based CO_2 capture from hydrogen production plants (productivities in the range of 60−90 $kg_{CO_2}/m^3/h$). The energy consumption, when evaluated via exergy to fairly compare heat and electricity, is in the range of state-of-the-art processes (0.5 MJ/kg CO_2). Finally, the developed VPSA cycles reduce the separation steps from two to one, which paves the way for further process intensification.

1. INTRODUCTION

Rapid and deep decarbonization of the global energy system is of the utmost importance: Limiting the global warming to 1.5 °C requires the world to reach net zero CO_2 emissions by 2050.[1] Carbon-neutral hydrogen is regarded as instrumental for such an energy system to enable the decarbonization of industry, transportation, and heating. However, it is very unlikely that the production of carbon-neutral hydrogen via electrolysis using renewable energy, so-called green hydrogen, will provide hydrogen at the required scale within the 2050 goal framework. At present, hydrogen is produced at rather large scale from fossil fuels, especially for use in refineries and production of chemicals, e.g., ammonia. Clearly, this production route features high CO_2 emissions and is not compliant with the 1.5 °C IPCC pathway. Accordingly, there is an urgent need for a scalable hydrogen production process that can already provide large quantities of hydrogen today with little associated CO_2 emissions.

Coupling fossil-fuel-based hydrogen production with carbon dioxide capture and storage (CCS) is likely the only route that can provide carbon-neutral hydrogen at the required scale and time. Moreover, it will accelerate the transition to a H_2-based energy system, with evident benefits for electrolyzer development. Finally, when replacing fossil fuels with biogenic sources, e.g., biogas, such technology will enable negative carbon emissions.

Different hydrogen production routes are shown in Figure 1. The state-of-the-art production from fossil fuels is autothermal

Received: May 23, 2019
Revised: July 23, 2019
Accepted: August 22, 2019
Published: August 22, 2019

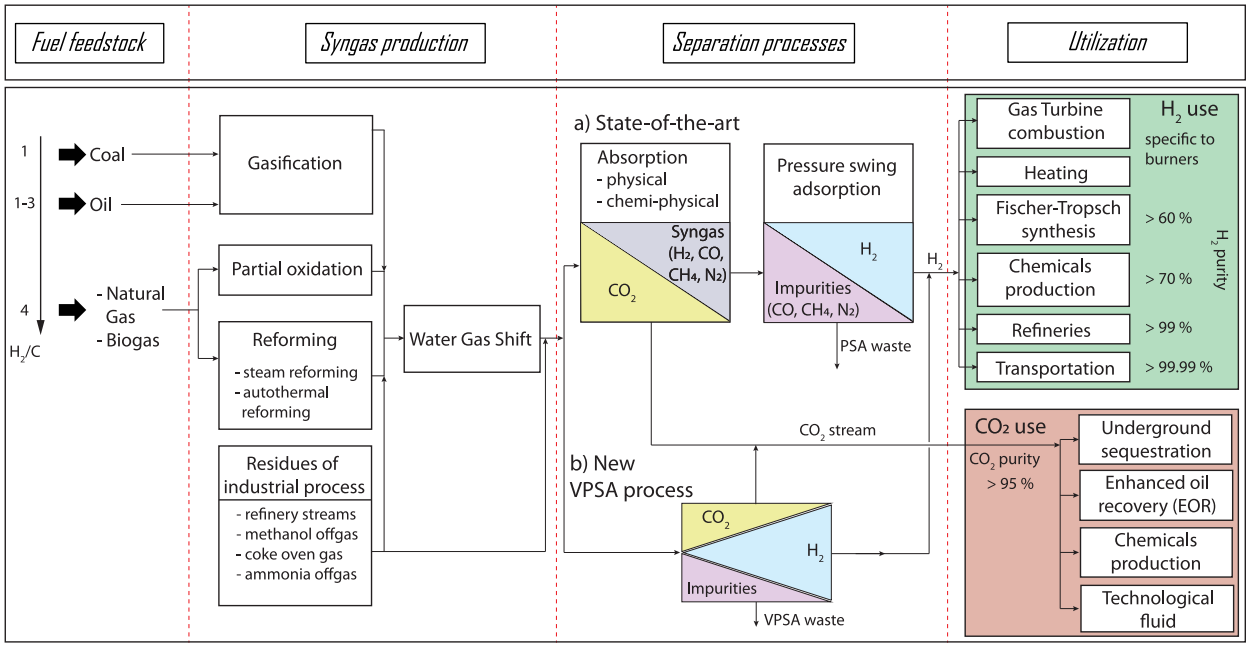

Figure 1. Fossil- and biofuel-based hydrogen production coupled with carbon capture using (a) state-of-the-art technology or (b) a new VPSA process.

or steam reforming of natural gas followed by a water−gas shift reactor to convert CO to CO_2. Alternatives include coal or oil gasification as well as partial oxidation of either natural gas or biogas. The different processes produce not only high-pressure syngas containing hydrogen and CO_2 but also significant amounts of impurities like N_2, CO, and CH_4. Therefore, the hydrogen production process requires a purification step, where H_2 is separated from CO_2 and impurities. The state-of-the-art process for this separation is a pressure swing adsorption (PSA) process, where a number of steps are used, including pressure equalizations, a product purge, and a product pressurization.[2] The process runs continuously by adopting several columns, often layered with different adsorbent materials. The final products are (i) a H_2 stream with purity sufficient for refineries or transportation and (ii) a waste stream.

Notably, such a configuration requires an additional unit to capture CO_2, e.g., before or after the PSA unit. Commercial processes for CO_2 capture exist and are based on absorption using aqueous solutions,[3] e.g., physical solvents (Selexol, Rectisol, or Purisol process) or hybrid chemical/physical solvents (activated MDEA, aMDEA). Other options include cryogenic separation, membranes, or adsorption.[4] In Figure 1, the state-of-the-art technology is shown with an absorption-based capture system before the PSA unit, which is the preferred option for coupling hydrogen production with CCS.[4] A promising alternative to these processes is the integration of hydrogen purification and CO_2 separation in a single adsorption cycle, i.e., what is shown as option b in Figure 1. By removing one separation stage, this will likely imply a decrease in complexity, system cost, and energy consumption. The development of advanced sorbents together with a high flexibility in terms of cycle design make adsorption processes suitable for a wide range of applications. However, adsorption processes for co-production of both light and heavy components, here H_2 and CO_2, respectively, have not been studied and developed thoroughly, and only a few examples exist in the literature. One such case is the Gemini process, which makes use of two interconnected PSA trains for the production of high-purity hydrogen and high-purity CO_2. Different adsorbents can be used in the different trains, and a vacuum pump is needed for CO_2 withdrawal.[5] The Gemini process, however, still uses two trains undergoing different cycles, which are only connected during specific steps. Notably, an industrial demonstration plant for CO_2 capture from a steam methane reforming (SMR) hydrogen production plant through adsorption exists at the Port Arthur refinery in Texas.[6] There, a vacuum swing adsorption (VSA) process is used to separate CO_2 from the syngas upstream of the PSA unit.[7]

The co-production of two products at high purities and recoveries involves many additional challenges compared to the purification of either the light or the heavy product. A suitable adsorbent selectively adsorbs CO_2 over impurities and hydrogen to allow for high-purity CO_2 product, while at the same time preferably adsorbing CO_2 and impurities over hydrogen to allow for high-purity hydrogen product. In addition to the availability of an appropriate adsorbent, performing this separation task within a single adsorption cycle requires the precise management of multiple concentration fronts. Because of the cyclic nature of adsorption processes, how fronts propagate in different steps is coupled in a complex manner. As a consequence, it is not sufficient to simply add steps typical for the purification of the light component to a cycle designed for the purification of the heavy component or vice versa; instead, new cycles have to be developed for different applications.

In this paper, we present an adsorption process for the co-production of hydrogen and CO_2 from a multicomponent feed within a single cycle. In particular, it presents the development and screening of different cycle configurations and the rigorous optimization of promising cycles to assess their separation performance, their energy requirement for a given separation task, and their effective productivity taking into consideration the scheduling in a multicolumn setup. Our main process

DOI: 10.1021/acs.iecr.9b02817
Ind. Eng. Chem. Res. 2019, 58, 17489−17506

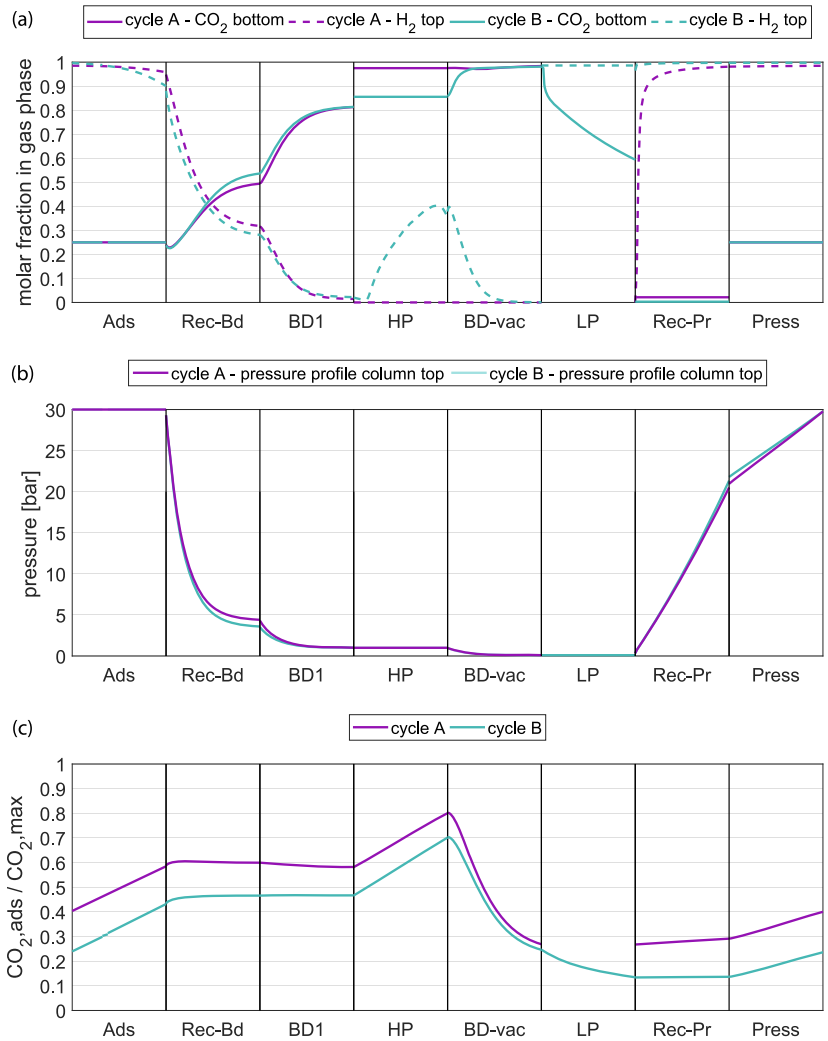

Figure 2. (a) Exemplary profiles of the molar fraction of CO_2 at the column bottom and H_2 at the column top over the normalized step duration for cycles A and B. (b) Exemplary pressure profiles at the column top over the normalized step duration for cycles A and B. (c) Ratio of CO_2 adsorbed to maximum possible CO_2 adsorbed at 1 bar (P_{HP}) and feed temperature over the normalized step duration for cycle A and cycle B. Cycle A does not have a light purge (LP) step; cycles C and D are conceptually similar to cycles A and B and show the same trends, with the pressure decreasing and increasing in sequence over three pressure-equalization (PE) steps replacing the recycling blowdown (Rec-BD) step and the pressurization with recycle (Rec-Pr) step. Ads, adsorption step; BD1, blowdown to heavy purge pressure; HP, heavy purge; BD-vac, blowdown to subatmospheric pressure.

target is hydrogen production with CCS, where both CO_2 and H_2 products should reach high purities and recoveries. Therefore, a recovery of ≥90% at purity of ≥95% for both products is pursued, which is in line with the recommendations of the United States Department of Energy for CO_2 capture rates[8] and CO_2 purity for transportation and storage in saline aquifers.[9,10] It is worth stressing that the process could be tuned for different specifications, e.g., higher purities with lower recoveries.

The structure of the paper is as follows. In the first section, the cycle design is explained, and four different cycles for the H_2−CO_2−impurity separation are introduced. In the second section, the column model is described, the important parameters are provided, and the optimization procedure is explained. In the third section, the separation and process performance of the different cycles is discussed explaining the influence of important process parameters, cycle configuration, and scheduling constraints on the key performance indicators, namely, the hydrogen and CO_2 purities and recoveries, the specific energy consumption, and the productivity. Finally, the most promising cycles are identified and compared to the state-of-the-art technology.

2. CYCLE DESIGN

The cycles for the H_2−CO_2−impurity separation presented here have been developed by combining in a new fashion the steps necessary to increase the purity or the recovery of either hydrogen or CO_2 or of both. These include high-pressure adsorption, recycling of hydrogen- and CO_2-rich streams for increasing recovery, purging with hydrogen and CO_2 to increase purity, and the use of different pressure levels for hydrogen, recycling, waste, and CO_2 withdrawal, including subatmospheric pressure. In addition to the purified hydrogen and CO_2 streams, an integrated adsorption process will produce a third stream containing the impurities together with residual H_2 and CO_2. The four most promising cycles are described below.[11] For the purposes of illustration, the evolution of the H_2 molar fraction at the column top and of

DOI: 10.1021/acs.iecr.9b02817
Ind. Eng. Chem. Res. 2019, 58, 17489−17506

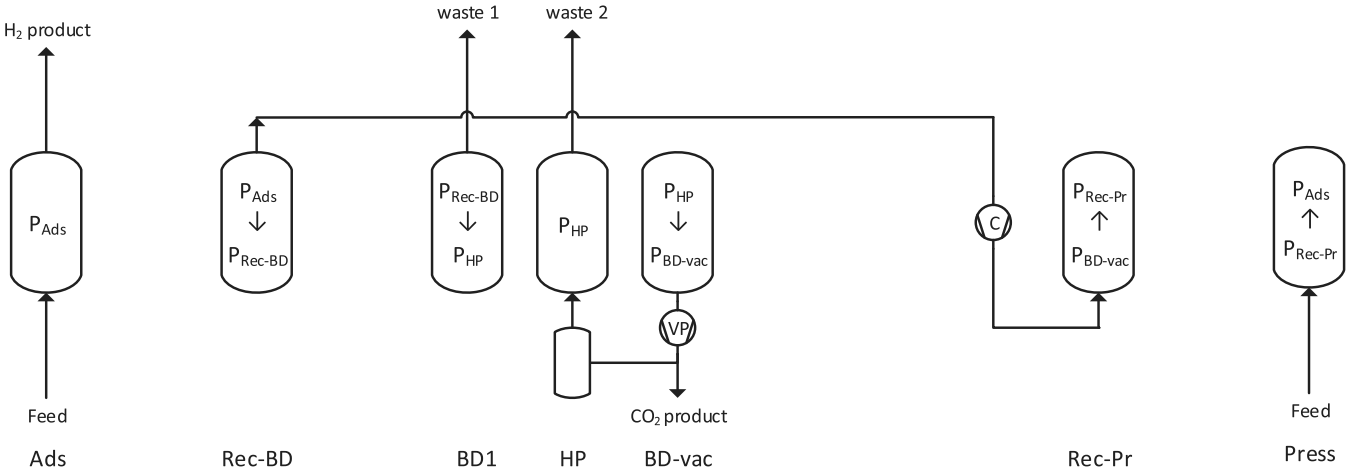

Figure 3. Cycle A: VPSA cycle for co-production of light and heavy product; compressor for recycle of hydrogen-rich stream.

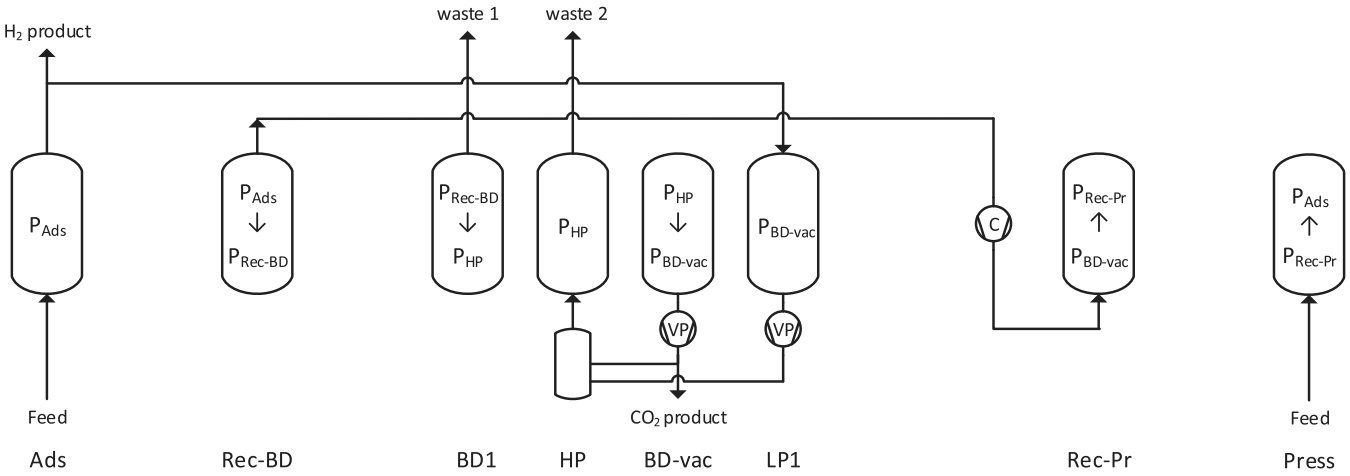

Figure 4. Cycle B: VPSA cycle for co-production of light and heavy product; compressor for recycle of hydrogen-rich stream, purge with hydrogen (LP), reduces to cycle A for $t_{LP1} \rightarrow 0$.

the CO_2 molar fraction at the column bottom over the course of one cycle at cyclic steady state (CSS) are shown in Figure 2a for representative simulations cycles A and B. The pressure profiles for the same simulations at the column top are shown in Figure 2b. In addition, the fractional CO_2 uptake, defined as the ratio of the amount of CO_2 adsorbed within the column to the amount that would be adsorbed if the whole column would be in equilibrium with CO_2 at the pressure of the heavy purge (HP), P_{HP}, is shown in Figure 2c. This illustrates the sorbent saturation with respect to CO_2 before the final evacuation. For further illustration, we refer to the internal gas-phase column profiles provided in the Supporting Information.

2.1. Cycle A. This cycle, shown in Figure 3, is a seven-step VPSA cycle combining most of the characteristic steps mentioned above. During a high-pressure adsorption step (Ads), hydrogen is produced at high purity, while impurity and CO_2 adsorb (see Figure 2). This is followed by a recycling blowdown step (Rec-BD), during which the column is depressurized to an intermediate pressure $P_{Rec\text{-}BD}$ and the outflow rich in hydrogen and impurity is recycled to partially repressurize the column before adsorption. This reduces the loss of H_2 while increasing its recovery. The Rec-BD is followed by a blowdown to heavy purge pressure (BD1), during which a waste stream lean in H_2 and rich in impurities is produced (see Figure 2). The column is then purged at constant pressure P_{HP} with part of the CO_2-rich product. During the HP, the impurities and the hydrogen, both in the adsorbed phase (mainly impurities) and in the gas phase, are replaced with CO_2. This increases the achievable CO_2 product purity, while more waste is produced. At the end of this step, the column is close to its maximum CO_2 adsorption capacity at P_{HP}, as shown in Figure 2c. This step is followed by a final blowdown to subatmospheric pressure (BD-vac), which is driven by a vacuum pump (VP). Here, the CO_2 product is withdrawn at high purity, as it can be seen in Figure 2a, and part of it is recycled and used for the HP step. In the subsequent two steps, the column is repressurized in a bottom up configuration, first with the recycled hydrogen-rich stream (Rec-Pr) using a compressor (C), and finally with the feed (Press), to reach the adsorption pressure, P_{Ads}.

2.2. Cycle B. A key drawback of cycle A is the large amount of CO_2 present within the column after the BD-vac step, as shown in Figure 2c. This reduces the achievable hydrogen purity and the CO_2 cyclic capacity, unless a very high vacuum is applied for regeneration. Therefore, in cycle B (Figure 4) a purge step is added after the BD-vac step, where the column is purged in a top down configuration with part of the light product (LP1, outow recycled to heavy purge), i.e., hydrogen. During this step, the column is cleaned starting from the top from adsorbed impurities and CO_2 while also displacing the

DOI: 10.1021/acs.iecr.9b02817
Ind. Eng. Chem. Res. 2019, 58, 17489−17506

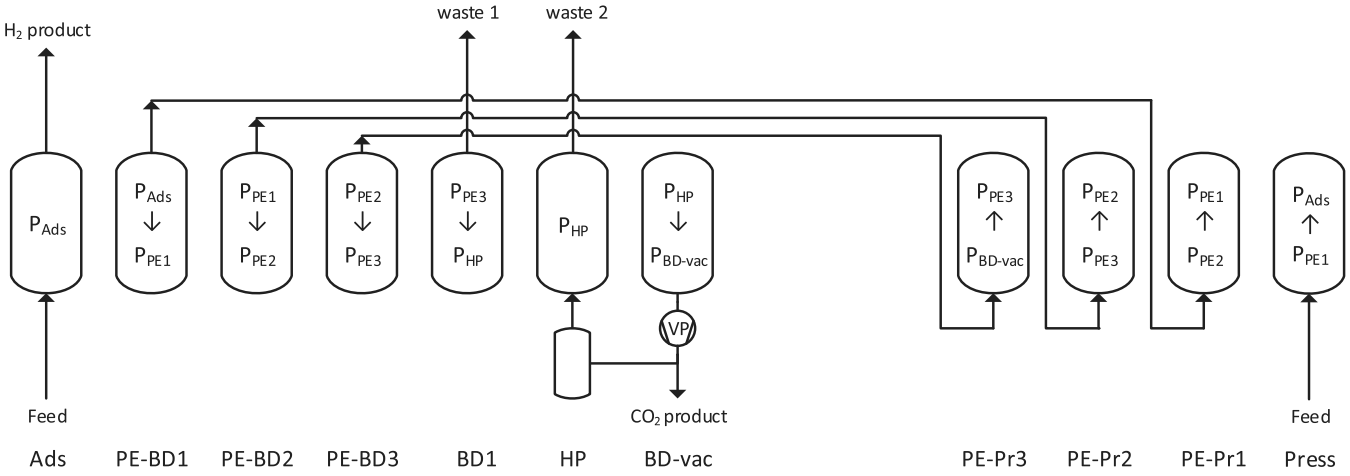

Figure 5. Cycle C: VPSA cycle for co-production of light and heavy product; three pressure equalizations for recycle of hydrogen-rich stream.

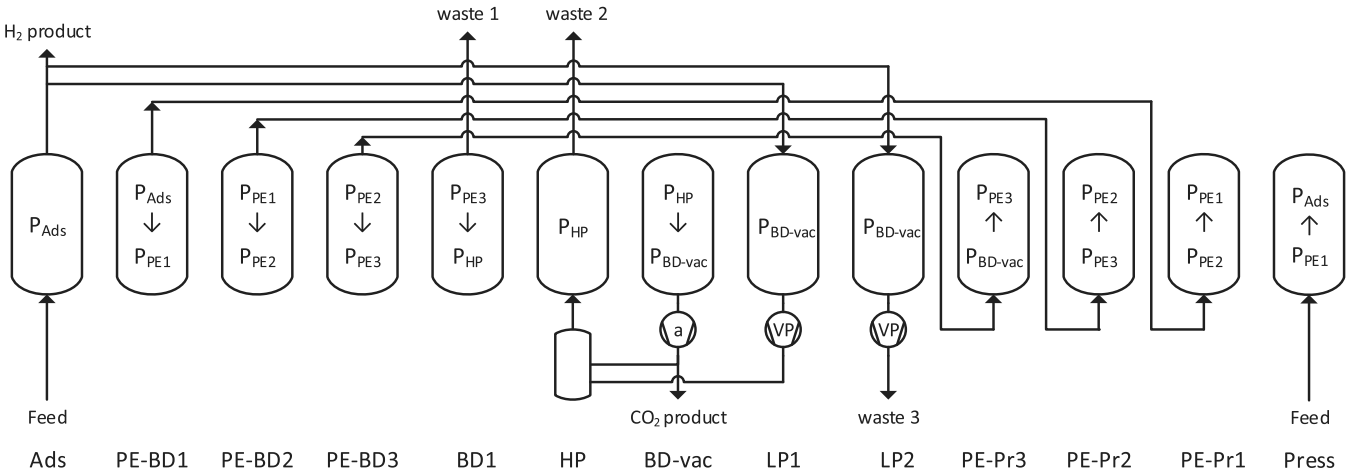

Figure 6. Cycle D: VPSA cycle for co-production of light and heavy product; three pressure equalizations for recycle of hydrogen-rich stream, purge with hydrogen, reduces to cycle C for $t_{LP1/2} \rightarrow 0$.

CO_2 in the void phase. The adsorbed CO_2 within the column decreases significantly, as illustrated in Figure 2c. A stream initially rich in CO_2 with increasing concentrations of impurities and hydrogen is produced, which is used as part of the stream used to purge the column in the HP step. Therefore, the CO_2 molar fraction of the HP inlet is lower compared to that of cycle A, as shown in Figure 2a, but hopefully still sufficient to successfully purge the column and withdraw high-purity CO_2 in the following step. The outflow of the HP step consists mostly of impurity with increasing amounts of hydrogen, which enters with the HP and is not adsorbed. This is different for cycle A, where no new hydrogen enters during the HP and the outflow consists mainly of impurity.

2.3. Cycle C. This cycle is shown in Figure 5 and is similar to cycle A with one conceptual difference regarding the methodology for recycling the hydrogen-rich intermediate product during the column depressurization. While cycle A uses a compressor, which provides high flexibility in terms of the final blowdown pressure but requires energy for recompressing the stream, cycle C adopts a series of three pressure equalization (PE) steps. This results in an 11 step cycle. A top-down configuration is chosen for all PE steps, in which the top of the column in the pressure equalization blowdown (PE-BD) step is connected with the bottom of the column in the pressure equalization pressurization (PE-Pr) step, to avoid contamination of the column top end with impurities. PE steps are expected to lower the energy consumption, while limiting the number of variables available for the fine tuning of the cycle.

2.4. Cycle D. Cycle D, which is shown in Figure 6, is based on cycle C, but features an additional LP step similar to cycle B, i.e., the possibility of venting the latter part of the outflow during the LP step (LP2). This could become necessary if the purge duration needed to reach the target hydrogen purity is very long. Then, the hydrogen and impurity content in the outflow of LP1 is too high for the HP step, hence it is wasted during LP2.

For adsorption processes, there is a trade-off between product purity and recovery. In the case of a ternary H_2/CO_2/impurity separation, where a waste stream is produced in addition to the two products, the purities and recoveries of CO_2-rich and H_2-rich product are not directly linked. Therefore, all these four indicators have to be taken into consideration for evaluating the separation performance. Notably, there are a few key design variables that strongly affect the performance of the different cycles.

2.5. Important Parameters. The duration of the adsorption step t_{Ads} has a strong influence on recovery and purity of both H_2 and CO_2. Increasing it leads to impurity and

DOI: 10.1021/acs.iecr.9b02817
Ind. Eng. Chem. Res. 2019, 58, 17489−17506

CO_2 fronts propagating further into the column, eventually contaminating the H_2 product and decreasing its purity. However, because of the longer duration of this step, more H_2 is produced during one cycle, which increases the H_2 recovery. For CO_2, the effect is opposite: longer adsorption times are favorable for its purity, but unfavorable for its recovery.

The HP step, as explained before, is mainly used to increase the CO_2 purity by replacing the gas phase rich in H_2 and impurities with a CO_2-rich gas phase. The variable influencing how much CO_2 is used for the HP is the recycle ratio *rr* of the BD-vac step, defined as ratio between the recycled to the total molar outflow of this step. Increasing the recycle ratio and using more of the CO_2 product for the HP step therefore leads to an increase in CO_2 purity. However, with higher recycle ratios more CO_2 is lost during the HP step and the CO_2 recovery decreases. Changing the recycle ratio has a strong influence neither on H_2 purity nor on its recovery.

The pressure, $P_{\text{Rec-BD}}$, is an important variable for cycles A and B to find the optimal trade-off between H_2 recovery and purity: Lower pressure increases the H_2 recovery because more H_2-rich outflow is recycled, but it decreases the H_2 purity because impurities and CO_2 build up at the end of this step, as shown in Figure 2a. Decreasing $P_{\text{Rec-BD}}$ therefore also leads to a slight increase in CO_2 recovery, but it has no significant effect on CO_2 purity.

Increasing P_{HP} leads to a decrease in CO_2 purity. First, because more hydrogen and impurities are contained within the column voids at the beginning of HP. Second, with reference to ambient pressure, more CO_2-rich recycled product is needed. For the same purge efficiency, stronger adsorption and higher gas density lead to slower propagation of the CO_2 front. For the same reason, less CO_2 is lost during this step, thereby increasing the CO_2 recovery with higher P_{HP}. The effect of the purge pressure on the hydrogen purity and recovery is small.

When maximizing the recovery or purity for one product while constraining the recovery and purity for the other, the effect of changing a variable on both products is relevant to reach the maximum for one but still be within the constraints for the other. It is clear from these considerations that the interplay among the different decision variables is not trivial, and a rigorous optimization approach is necessary to obtain the best separation and process performance for the different cycle configurations, as explained in the next section.

3. PROCESS MODELING AND OPTIMIZATION

3.1. Mathematical Model. A nonisothermal, one-dimensional model based on mass, energy, and momentum balance equations is used for modeling the process. It has previously been validated for a variety of conditions and cycles[12−14] and has been extensively used for the design of new cycles.[15,16] The equations are provided in the Supporting Information, the main simplifications and assumptions are summarized here: (1) There are no radial gradients in concentration, velocity, and temperature. (2) The Ergun equation is used to describe the pressure drop along the column. (3) Thermal equilibrium exists between the gas phase and the solid phase. (4) The gas phase is described using the ideal gas law,[17] which is a well-accepted simplification for VPSA simulation. As reference, the compressibility factor for the $CO_2/N_2/H_2$ mixtures calculated with Refprop 9.0 is between 0.95 and 1.00 for the pressures and temperatures of interest. (5) Mass transfer is described using a linear driving force approximation, and a temperature/concentration independent mass transfer coefficient. (6) Axial dispersion and conductivity are neglected.[12] (7) The heat of adsorption, molar heat capacities, and viscosity of the gas phase are constant.

For modeling the cyclic nature of adsorption processes, a single column is simulated that cyclically undergoes the sequence of steps by changing the boundary conditions until a CSS is reached. At CSS, neither the internal composition and temperature profiles nor the product composition and the total mass balance change between two consecutive cycles, as described in detail in previous work.[15,16,18] The threshold for the mass balance is set to below 1% for cycles A and B and below 2% for cycles C and D (due to the PE steps), and the threshold for the internal profiles to 10^{-4}. The pressure decrease during BD steps is described as exponential decay in the following form:

$$P(t_s) = P_{\text{low}} + (P_{\text{high}} - P_{\text{low}}) \exp(-\xi t_s) \tag{1}$$

A value of $\xi = 0.11$ is used in this work. ξ has been fitted to cyclic experiments under similar conditions, as discussed by Marx et al.[19] An intermediate storage tank is assumed to be present for all recycling steps and adiabatic operation is assumed for the columns.[18]

Activated carbon (AC) was identified as promising adsorbent for the considered separation and is used for all simulations. We do not expect this to be the optimal choice for all applications, but we want to keep our analysis general and leave the choice of the best adsorbent or adsorbent combination to specific case studies. In addition, this allows us to profit from a very good experimental database for AC in terms of single component and binary isotherms for CO_2, N_2, and H_2 as well as mass transfer parameters from binary and ternary breakthrough experiments.[17,19,20] The adsorption equilibria, which have previously been characterized in our group, are described in the form of a temperature-dependent multicomponent Sips isotherm. The equations and isotherm parameters are reported in the Supporting Information. The other relevant parameters are provided in Table 1.

A generic inlet consisting of 50% CO_2 and 25% H_2 as well as 25% N_2 as impurity at a pressure of 30 bar is used for cycle screening and optimization. Here, the aim is to design and identify cycles that can provide high-purity and -recovery CO_2 and H_2 in the presence of significant amounts of impurities. Typically, syngas impurities, e.g., CO, N_2, and CH_4, adsorb more than H_2 but less than CO_2. Moreover, they usually account for 5−10 vol % of the feed gas. In this work, we have decided to represent all impurities with a large molar fraction of N_2, a condition for which the model has been validated experimentally.[13]

In addition to the impurities mentioned above, which are typically present in % or ‰ levels, several trace impurities like higher hydrocarbons or sulfur components can be present in the feed at much lower concentrations down to ppm levels, depending on the upstream process. A common feature of those trace impurities is that they adsorb stronger and often irreversibly on adsorbents like AC or zeolites. Therefore, a guard layer is usually included in the column to reversibly adsorb the trace impurities and protect the main part of the bed. For this general analysis, we do not consider a guard layer, because it depends on the nature and concentration of those trace impurities, which are process-specific. However, a few considerations as to how the design of the cycles presented above influences such a guard layer should be made. Several of

DOI: 10.1021/acs.iecr.9b02817
Ind. Eng. Chem. Res. 2019, 58, 17489−17506

Table 1. Material and Column Parameters for the Simulations[a]

parameter	symbol	unit	value
particle diameter	d_p	m	0.003
material density	ρ_M	kg/m^3	1965
particle density	ρ_P	kg/m^3	850
bed density	ρ_b	kg/m^3	480
heat capacity adsorbent	C_s	J/kg/K	1000
isotherm parameters	see the Supporting Information, as reported in ref 20		
isosteric heat of adsorption	$\Delta H_{Ads,i}$	J/mol	CO_2: 21000; N_2: 15600; H_2: 9800
mass transfer coefficient	k_i	1/s	CO_2: 0.11; N_2: 0.3; H_2: 1[b]
Internal column diameter	d_i	m	0.025[c]
column length	L_{col}	m	1.2[c]

[a]Details in Marx et al[13]. [b]Fitted to breakthrough experiments for a ternary mixture equivalent to the one used for this study: $H_2/CO_2/N_2$ = 50:25:25. [c]Based on lab-scale adsorption setup at ETH Zurich.

the recycled streams (PE-Pr, HP, and Rec-Pr) are directed to the column top, thereby possibly leading to a further propagation of the impurities into the column bed. Therefore, an external guard bed might be a more suitable solution for the presented cycles. Alternatives include a longer guard bed or feeding the recycle streams on top of the guard layer.

Water, which on AC adsorbs more than CO_2 if the relative humidity is large enough (about 25−30%), is also usually present in traces in pressurized syngas at ambient temperature, as relevant here. Its strong adsorption, hysteresis behavior, and competition with CO_2 make the quantitative description within simulation of CSS processes particularly challenging. The H_2O adsorption behavior on AC, and related challenges, were extensively discussed by Hefti and Mazzotti.[21,22] Examples in the literature where H_2O is considered in cycle simulations are scarce and typically refer to the use of layered beds in the context of postcombustion CO_2 capture, where water is a prominent impurity.[16,23,24] Moreover, H_2 purification from wet syngas is current industrial practice in PSA. Accordingly, in this work we do not consider H_2O in the feed to the VPSA, which is assumed to be perfectly dry.

3.2. Key Performance Indicators. The most important indicators to compare the separation performance of different adsorption processes are the product purities and recoveries. The purity Φ_i is defined as the ratio between the amount of moles of target component i in the product rich in this component, $N_{i,Prod}$, to the total amount of moles of this product, $N_{tot,Prod}$:

$$\Phi_i = \frac{N_{i,Prod}}{N_{tot,Prod}} \tag{2}$$

The recovery r_i is defined as the ratio of $N_{i,Prod}$ to the overall amount of component i fed to the cycle, $N_{i,tot}$, as follows:

$$r_i = \frac{N_{i,Prod}}{N_{i,tot}} \tag{3}$$

Two additional parameters are used to characterize the process performance for a given separation, namely the specific energy consumption e and the effective productivity Pr_{eff}. Whereas the specific energy consumption is an indicator of the operating cost of the plant, the productivity determines the total plant volume, a major contributor to the capital cost, and the amount of adsorbent needed, which is part of the operating cost. The specific energy consumption is given per mass of product i separated (CO_2 or hydrogen) in kJ/kg, and the effective productivity as mass of product separated per unit time and unit mass of adsorbent in kg/(t_{ads}h):

$$e = \frac{E_{tot}}{N_{i,Prod} M_{w,i}} \tag{4}$$

$$Pr_{eff} = \frac{N_{i,Prod} M_{w,i}}{(t_{cycle} + t_{idle})\rho_b V_{col}} \tag{5}$$

where $M_{w,i}$ is the molecular weight of component i, ρ_b is the bulk density, and V_{col} is the column volume.

To compute the total energy consumption of the VPSA process E_{tot}, three different contributions must be considered: (1) the energy required by the VP for evacuating and purging the column at $P < P_{Amb}$, E_{VP}, (2) the energy required to compress the recycled part of the CO_2 product from ambient pressure to P_{HP}, in case HP is carried out above ambient pressure, E_{HP}, and (3) the energy required for recompressing the hydrogen-rich stream, E_{H_2}.

Ultimately, all three energy needs are requested in the form of electricity to drive the three corresponding machines. In addition, the separation process might affect the downstream product compression, e.g., the CO_2 compression for geological storage or the H_2 compression for ammonia production or any other further use. This would be particularly relevant if (i) the products pressure varies when changing the cycles variables and/or (ii) H_2 and/or CO_2 are supplied at different pressures compared to those in the state-of-the-art process, e.g., CO_2 above P_{Amb} or H_2 at $P < P_{Feed}$. However, for all four cycles considered here, the two products leave the VPSA at constant pressure irrespective of the changes in the considered design variables and are in line with the state-of-the-art processes, i.e., CO_2 at P_{Amb} and H_2 at about P_{Feed}. Accordingly, the products compression is not considered in our optimization as this would result in a constant demand, equal to the state-of-the-art process and dependent on the downstream process, which is not included as part of this work.

The computation of the three energy contributions is based upon simple isoentropic efficiency η_{is} or more detailed models in Aspen Plus, specifically: (i) For E_{VP}, we assume a linear stepwise decrease in the vacuum pump efficiency for decreasing vacuum pressure, which is required to account for lower performance at deeper vacuum conditions, as shown in Krishnamurthy et al.[25] (ii) E_{HP} is computed with a constant η_{is} = 0.8. (iii) E_{H_2} is computed using a polynomial regression of an intercooled compression simulated in Aspen Plus, where the input variables are the total compression ratio and the H_2 content in the recycle. Notably, the latter allows to consider the changing composition and pressure ratio in the H_2-rich recycle.

Because of the cyclic nature of adsorption processes, they are usually accommodated in a series of columns executing the same sequence of steps shifted in time. To synchronize steps like pressure equalizations which require the direct connection

DOI: 10.1021/acs.iecr.9b02817
Ind. Eng. Chem. Res. 2019, 58, 17489−17506

Table 2. Cycle Parameters and Variables for Optimization of CO_2 and H_2 Separation Performance and Parametric Analysis of Energy Consumption and Productivity

		Process Conditions							
		separation performance				energy/productivity			
cycle	unit	A	B	C	D	A	B	C	D
T_{feed}	K	298				298			
P_{Ads}	bar	30				30			
$\dot{V}_{feed}$[a]	m^3/s	2×10^{-5}				2×10^{-5}			
$P_{BD\text{-}vac}$	bar	0.1[b]	0.1			$f(t_{BD\text{-}vac})$[c]			
$y_{i,feed}$[d]		$H_2/CO_2/N_2$ = 50:25:25				$H_2/CO_2/N_2$ = 50:25:25			
t_{Ads}[e]	s	variable				variable			
$t_{Rec\text{-}BD}$	s	50		—		variable		—	
$P_{Rec\text{-}BD}$	bar	variable		—		$f(t_{Rec\text{-}BD})$[c]		—	
t_{BD1}	s	50				50			
t_{HP}	s	50				50			
$t_{BD\text{-}vac}$	s	50				variable			
t_{LP1}	s	—	$f(t_{Ads,LP1/2})$[f]	—	$f(t_{Ads,LP1/2})$[f]	—	$f(t_{Ads,LP1/2})$[f]	—	$f(t_{Ads,LP1/2})$[f]
t_{LP2}	s	—			$f(t_{Ads,LP1/2})$[f]	—			$f(t_{Ads,LP1/2})$[f]
$t_{Rec\text{-}Pr}$	s	30		—		30		—	
$t_{PE\text{-}Pr/PE\text{-}BD}$	s	—		5		—		5	
rr		variable				variable			

[a]Defined at P_{Feed} and T_{Feed}. [b]Optimization of CO_2 separation performance for different pressure levels $P_{BD\text{-}vac}$ from 0.01 to 0.3 bar; see Figure 8. [c]Exponential pressure decrease according to eq 1. [d]Cycle A: Optimization of CO_2 separation performance for two additional impurity contents: $H_2/CO_2/N_2$ = 46.7:23.3:30 and $H_2/CO_2/N_2$ = 53.3:26.7:20; see Figure 8. [e]Including pressurization and the time dedicated to provide the hydrogen for the purge LP1/2. [f]Depending on duration of adsorption step during which the outflow hydrogen product is used to purge the column, $t_{Ads,LP1/2}$: $t_{LP1/2} = 50 \times t_{Ads,LP1/2}$.

of two columns, or to fulfill additional process constraints, e.g., a continuous feed flow, or a continuous production, an idle time t_{idle} is necessary. The idle time depends on the cycle configuration, the step times, and the number of columns N_{col} used. Notably, a minimum number of columns $N_{col,min}$ is necessary to accommodate a specific cycle under specific constraints, yet the optimal number of columns can be higher if this allows for a significant reduction of idle times. The effective productivity Pr_{eff} can differ significantly from the productivity for an infinite number of columns resulting in zero idle times $Pr_{inf} = Pr_{eff}$ ($t_{idle} = 0$). Whereas the one-column model used in this paper computes the productivity for an infinite number of columns, the effective productivity used to compare different cycles Pr_{eff} as defined in eq 5 takes the scheduling and resulting idle times into account. The scheduling equations needed to calculate the idle time for different cycle configurations are provided in the Supporting Information. The constraints are a synchronization of the PE steps and a continuous feed.

3.3. Optimization and Parametric Analysis. *3.3.1. Separation Performance.* For optimizing the separation performance, the code is combined with a multiobjective optimization routine. The optimization is based on a multilevel coordinate search (MCS) algorithm that was adapted to handle multiple objectives (MO-MCS) as described in Capra et al.[26] The variables considered in the optimization are P_s pressures and durations t_s of each of the different steps, s, whereas adsorbent and column related parameters are kept constant. Because of the many steps and different pressure levels, only parameters with a strong influence on the cycle performance are included in the optimization. Those are listed below for all considered cycles: **Cycle A**: (i) the duration of the adsorption step, t_{Ads}, (ii) the pressure at the end of the Rec-BD step, $P_{Rec\text{-}BD}$, and (iii) the recycle ratio rr of the BD-vac step. **Cycle B**: The same parameters as for cycle A are optimized, as well as (i) the duration of the LP1 step and (ii) the amount of hydrogen used for this step. **Cycle C**: (i) the duration of the adsorption step, (ii) the recycle ratio, and (iii) the pressure at which the high pressure purge is carried out, P_{HP}. **Cycle D**: The decision variables are the same as for cycle C. Also included are (i) the duration of both LP1 and LP2 and (ii) the amount of hydrogen used for those steps as described for cycle B.

To assess the separation performance, two different optimizations are carried out for all cycles with the decision variables vector $\mathbf{x}$ as mentioned above:

Optimization separation performance CO_2:

$$\underset{\mathbf{x}}{\text{minimize}} \quad (-\Phi_{CO_2}(\mathbf{x}), -r_{CO_2}(\mathbf{x}))$$
$$\text{s.t.} \quad r_{H_2} \geq 0.90$$
$$\Phi_{H_2} \geq 0.95$$

Optimization separation performance H_2:

$$\underset{\mathbf{x}}{\text{minimize}} \quad (-\Phi_{H_2}(\mathbf{x}), -r_{H_2}(\mathbf{x}))$$
$$\text{s.t.} \quad r_{CO_2} \geq 0.85$$
$$\Phi_{CO_2} \geq 0.95$$

A constraint of 85% was chosen for the CO_2 recovery for the optimization of the H_2 separation performance, because not all cycles did reach 90% while delivering a CO_2 purity ≥95%. This allows us to assess the influence of the different variables on both purities and recoveries and to compare the different cycle configurations. The decision variables, steptimes, pressure levels, and feed streams considered for all simulations are provided in Table 2.

DOI: 10.1021/acs.iecr.9b02817
Ind. Eng. Chem. Res. 2019, 58, 17489−17506

3.3.2. Energy Consumption and Productivity. To assess the energy consumption and productivity, an extensive parametric analysis was carried out. With this approach, the constraints on hydrogen and CO_2 recoveries and purities do not need to be defined beforehand, and the optimal performance of the different cycles can be compared for different purity and recovery constraints. To obtain the same level of refinement for the Pareto front as with the optimizer, however, significantly more function evaluations would be necessary. Therefore, first a coarse parametric analysis is carried out which is subsequently refined for the promising ranges of different decision variables.

The decision variables are the same as for the optimization of the separation performance. In addition, also the duration of the BD-vac step is set as variable thereby also varying the lowest column pressure. The lowest pressure P_{low}, as defined in eq 1, is 0.01 bar. In accordance with this, and for the Rec-BD step, the duration $t_{Rec\text{-}BD}$ is set as variable instead of defining the final pressure $P_{Rec\text{-}BD}$. This allows to include the impact of the step duration on the productivity. The decision variables, step times, pressure levels, and feed stream condition for all simulations are provided in Table 2.

4. RESULTS AND DISCUSSION

In this section we will show the following: which cycles and which among their features are favorable for reaching a good CO_2 separation performance; which cycles and which among their features are favorable for reaching a good H_2 separation performance; which cycles can achieve the desired co-production of both products and at what energy penalty and productivity; and how the most promising cycles perform compared to state-of-the-art absorption processes for CO_2 capture from H_2 production facilities.

The four cycles can be categorized as indicated in Table 3. Cycle A as a base cycle has no LP step and makes use of a compressor for recycling part of the hydrogen-rich outflow. Cycle B has an additional LP step. Cycle C is based on cycle A but makes use of PE steps for recycling part of the hydrogen-rich outflow instead of a compressor, and cycle D has both a LP step and PE steps. Therefore, the effect of the LP step and of exchanging a compressor with a series of PE steps can be assessed separately.

Table 3. Four Different Cycles Developed for CO_2−H_2 Co-Production

	with compressor	with PE steps
without LP	cycle A	cycle C
with LP	cycle B	cycle D

Whereas we expect the LP step to have a positive influence on the CO_2 cyclic capacity, it might result in a lower CO_2 purity, because of the increasing amount of impurity in the purge gas for the HP step. In section 4.1, we will show that the influence on the CO_2 separation performance is indeed positive and that CO_2 can be produced at a sufficient purity. Exchanging a compressor with PE steps translates not only into a loss of flexibility and therefore possibly of separation performance but also into savings in energy consumption. We will show in section 4.1 that the influence on the CO_2 separation performance is marginal, whereas the H_2 separation performance decreases significantly when making use of PE steps instead of a compressor. For the desired product purities and recoveries, however, PE steps are sufficient and result in a reduced energy penalty compared to using a compressor, as will be shown in section 4.2.

The section starts by examining the effect of different factors on the separation performance, including the cycle configuration, the feedstream composition and the evacuation pressure. Subsequently, the energy consumption and productivity for the different cycles will be compared including the effect of scheduling on productivity. Finally, the different cycles will be compared to the state-of-the-art technology based on their overall performance and their suitability for different applications.

4.1. Optimization: Separation Performance. Figure 7 shows the Pareto fronts for the four different cycles when (a) maximizing CO_2 recovery and purity while co-producing high-purity and -recovery hydrogen and (b) maximizing H_2 recovery and purity while co-producing high-purity and -recovery CO_2 with parameters and variables as shown in Table 2.

4.1.1. Influence of Cycle Configuration on CO_2 Purity and Recovery. Figure 7a shows that CO_2 can be produced at very high purity (>99.7%) or at very high recovery (>99%) for all cycles while co-producing H_2 at high-purity and -recovery specifications. The target of ≥95% CO_2 purity and ≥90% CO_2 recovery, however, can only be reached for two cycles, cycles B and D, whereas cycles A and C miss the target region by a few percentage points. The figure shows clearly that cycles A and C as well as cycles B and D have very similar performances in terms of CO_2 purity and recovery.

4.1.1.1. Compressor versus PE. The main difference between cycles A and C (or between cycles B and D,

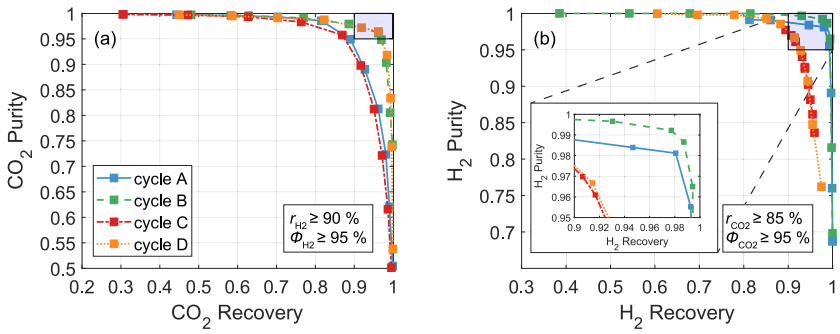

Figure 7. Separation performance for all cycles: (a) CO_2 purity and recovery for different cycles, constraints: ≥90% H_2 recovery, ≥95% H_2 purity. (b) H_2 purity and recovery for different cycles, constraint: ≥85% CO_2 recovery, ≥95% CO_2 purity.

DOI: 10.1021/acs.iecr.9b02817
Ind. Eng. Chem. Res. 2019, 58, 17489−17506

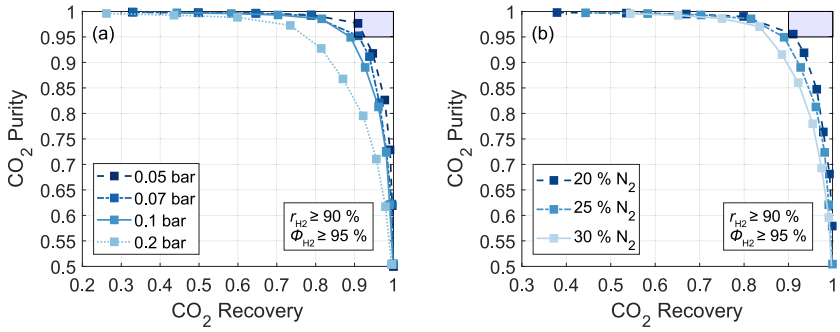

Figure 8. Optimized separation performance for cycle A: maximized Φ_{CO_2} and r_{CO_2} for different cycles, constraints: $r_{H_2} \geq 90\%$, $\Phi_{H_2} \geq 95\%$. (a) Different evacuation pressures at $y_{N_2} = 25\%$. (b) Different impurity content in the feedstream at $P_{BD\text{-}vac} = 0.1$ bar; when decreasing/increasing y_{N_2}, the ratio of CO_2 to H_2 was kept constant.

respectively) is the way the hydrogen is recycled: with a compressor in the case of cycles A and B, while exploiting PE steps for cycles C and D. The difference in the CO_2 purity/recovery is small for cycles that only differ in the way the hydrogen is recycled. This shows that pressure at the end of the hydrogen recycle ($P_{Rec\text{-}BD}$ or $P_{PE\text{-}BD3}$ respectively) has only a minor influence on the CO_2 purity and recovery. In addition, for a large part of the Pareto front, the optimal pressure at the end of the Rec-BD reached when using a compressor is close to the final pressure reached after the third PE-BD step (4−5 bar). The possibility of fine-tuning the Rec-BD pressure for cycles A and B therefore does not have a significant effect on the CO_2 separation performance.

4.1.1.2. LP Step. In contrast to the small influence of exchanging the compressor for PE steps, the addition of a LP step to either cycle A or C increases significantly the separation performance with respect to CO_2, which can now be obtained at high purity with high recovery (approximately 97% CO_2 recovery for 95% CO_2 purity possible). During the LP step, hydrogen replaces CO_2 within the gas phase. This leads to additional CO_2 desorption, which is withdrawn from the column at relatively high purity. Because the CO_2-rich outflow is recycled and used to purge the column in the HP step, the LP increases the effective cyclic CO_2 capacity. Less product CO_2 has to be used for the same HP efficiency, thus resulting in a higher recovery at the same purity. For cycle D, the option of wasting part of this outflow has also been included in the optimization. This, however, has a negative effect on the CO_2 recovery because part of the CO_2 is wasted and has only a minor effect on the CO_2 purity. Therefore, the duration of this purge is very small for all optimal points.

4.1.2. Influence of Cycle Configuration on H_2 Purity and Recovery. Figure 7b illustrates the optimization of the hydrogen purity and recovery. To be able to compare all cycles, a constraint of ≥85% CO_2 recovery together with ≥95% CO_2 purity was chosen. The Pareto sets show clearly that all cycles can easily produce high-purity hydrogen at high recovery, i.e., surpassing the target of ≥90% H_2 recovery and ≥95% H_2 purity. A very high-purity hydrogen product (>99.97%) can be produced with cycle B or D including the LP step, whereas very high hydrogen recovery (>99.96%) can be reached for cycles A and B, which make use of a compressor for recycling the hydrogen-rich blowdown outflow. Thus, both the LP step and the way the hydrogen-rich outflow is recycled after the adsorption step strongly affect the hydrogen separation performance.

4.1.2.1. Compressor versus PE. Whereas the final pressure at the end of the Rec-BD step (relevant for cycles A and B) has only a minor effect on both CO_2 recovery and purity, it is an important variable to find the optimal trade-off between H_2 recovery and purity: Lower pressure leads to an increase in hydrogen recovery, because more hydrogen-rich outflow is recycled, and to a decrease in hydrogen purity, because more impurities and more CO_2 are recycled. For very high H_2 recoveries, the pressure $P_{Rec\text{-}BD}$ approximates the minimum possible pressure at the end of this step, P_{HP}, thus making the intermediate BD1 unnecessary. When using PE steps instead of a compressor, the final pressure at the end of PE-BD3 is determined mainly by the number of PE steps. In developing cycles C and D, three PE steps have been identified as favorable for achieving the target CO_2 purity and recovery while limiting the complexity. The final pressure after PE-BD3 is in the range of 4−5 bar, which is significantly higher than P_{HP}, and therefore limits the maximum hydrogen recovery for cycles C and D. Increasing the number of PE steps would lead to an increase not only in performance (hydrogen recovery), but also in the minimum number of columns and valves required.

For maximizing hydrogen purity, increasing $P_{Rec\text{-}BD}$ (or reducing the number of PE steps) is required, because less impurities are recycled. Therefore, cycle A reaches higher purities than does cycle C. However, the addition of the LP step allows high-purity hydrogen production for both cycles B and D as discussed below. It should be noted that the influence of $P_{Rec\text{-}BD}$ on purity is significantly lower than on recovery.

4.1.2.2. LP Step. The LP step is not only beneficial for the CO_2 separation performance, but it also increases the maximum obtainable hydrogen purity significantly, which is clear when comparing the H_2 Pareto fronts of cycles A and B (or of cycles C and D). The LP step results not only in the desorption of additional CO_2 but also in the effective removal of CO_2 and impurities from the column top, thus pushing the obtainable hydrogen purity to above 99.97% for cycles B and D. This step, however, uses part of the H_2 product, thus decreasing its recovery. For high target hydrogen recovery, the duration of the purge approximates zero and cycles B and D reduce to cycles A and C, respectively: The Pareto fronts overlap. Cycle B, which combines the two favorable features for the production of high-purity hydrogen at high recovery, namely, the Rec-BD with compressor and the LP, achieves a hydrogen product purity of 99.9% with a recovery of 90% while co-producing CO_2 at recovery ≥85% and purity ≥95%.

DOI: 10.1021/acs.iecr.9b02817
Ind. Eng. Chem. Res. 2019, 58, 17489−17506

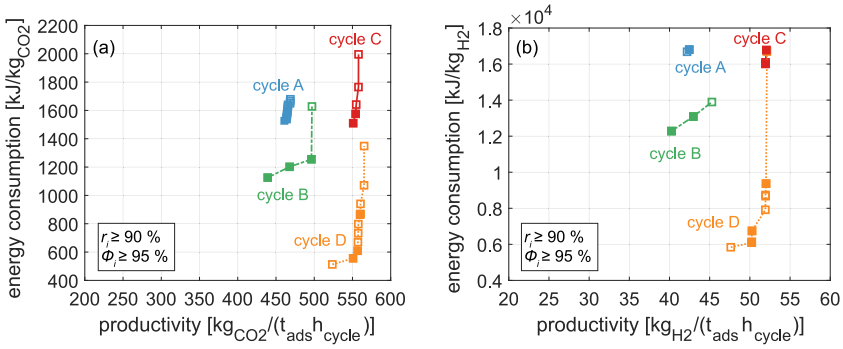

Figure 9. Optimized (parametric analysis) energy consumption and productivity for all cycles, constraints: $r_{H_2} \geq 90\%$, $\Phi_{H_2} \geq 95\%$, $r_{CO_2} \geq 90\%$, $\Phi_{CO_2} \geq 95\%$. (a) Per CO_2 separated; (b) per hydrogen produced. Points representing an optimum for both products are represented as filled symbols, and those only representing an optimum for either CO_2 or H_2 are represented as empty symbol.

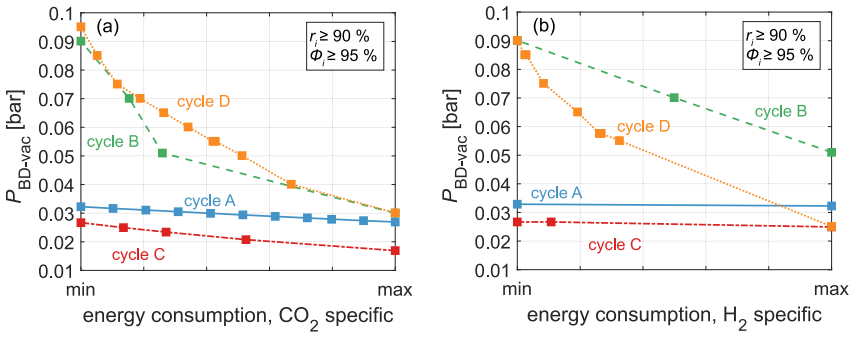

Figure 10. Change of evacuation pressure $P_{BD\text{-}vac}$ moving along Pareto front from minimum to maximum CO_2 specific energy consumption (a) and from minimum to maximum H_2 specific energy consumption (b). Constraints: $r_{H_2} \geq 90\%$, $\Phi_{H_2} \geq 95\%$, $r_{CO_2} \geq 90\%$, $\Phi_{CO_2} \geq 95\%$.

4.1.3. Influence of Evacuation Pressure and Impurity Content on CO_2 Purity and Recovery. In addition to the cycle decision variables discussed above, there are two boundary conditions that strongly affect the separation performance: (i) the final evacuation pressure $P_{BD\text{-}vac}$ and (ii) the molar fraction of the impurity in the feed, y_{N_2}. We have therefore investigated how different values influence the CO_2 separation performance, by considering cycle A as an exemplary test case. It should be mentioned that the H_2 separation performance follows similar trends. The results are illustrated in Figure 8, which shows the change of the Pareto fronts when changing the evacuation pressure (Figure 8a) and the N_2 content in the feed (Figure 8b).

4.1.3.1. Evacuation Pressure. With lower evacuation pressure, the cyclic CO_2 capacity increases because more CO_2 desorbs and can be recovered as product during the evacuation. This leads to an increase in CO_2 recovery for the same purity. In fact, lowering the minimum evacuation pressure to 0.07 bar enables cycle A to reach the targeted CO_2 purity and recovery (95 and 90%, respectively). It is worth stressing that a lower evacuation pressure is favorable for the separation performance but leads to a higher energy consumption, as more energy is required for the vacuum pump. Therefore the evacuation pressure is an important decision variable for the optimization of energy consumption and productivity. Notably, with the evacuation pressure as additional variable, all cycles can reach >90% recovery for both products at >95% purity. Decreasing the evacuation pressure also has a positive effect on the hydrogen separation performance: The higher cyclic capacity for CO_2 results in a longer duration of the adsorption step before the nitrogen front breaks through, which leads to an increase in hydrogen recovery for the same hydrogen purity.

4.1.3.2. Impurity Content. When reducing the N_2 content, which plays the role of impurities in our calculations, the CO_2 in the adsorbed phase and in the gas phase increases, which makes the separation easier. For the hydrogen separation, reducing the impurity content is also favorable: Under the operating conditions of interest, the convex isotherm shape allows for prompt N_2 adsorption while limiting the N_2 content in the gas phase significantly. Therefore, the propagation velocity of the impurity front decreases with a decreasing impurity content. This allows for a longer adsorption step before the nitrogen front breaks through. This leads to increasing hydrogen recovery while maintaining the same hydrogen purity. For an increase in N_2 concentration in the feed, the separation performance gets worse, based on the same argument.

4.2. Parametric Analysis: Energy Consumption and Productivity. *4.2.1. Cycle Comparison.* The results of the parametric analysis for minimizing energy consumption and maximizing ideal productivity, i.e., considering zero idle time, by varying operating variables as shown in Table 2 are illustrated in Figure 9 in the form of Pareto fronts, considering both CO_2 (Figure 9a) and H_2 (Figure 9b) as products. Notably, the Pareto points might differ depending on the target product, i.e., CO_2 or H_2. This is because the recovery and purity of the CO_2 and hydrogen product can differ along the Pareto front, as long as they satisfy the minimum constraint. Points representing a Pareto optimum for both products are indicated as filled symbols, those representing an

DOI: 10.1021/acs.iecr.9b02817
Ind. Eng. Chem. Res. 2019, 58, 17489−17506

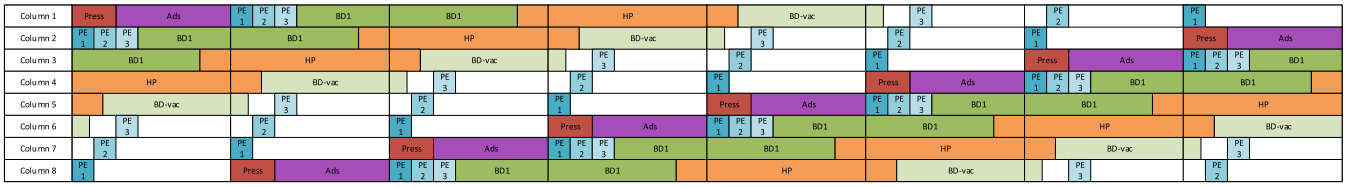

Figure 11. Schedule for cycle C for the minimum CO_2-specific energy consumption and the minimum number of columns (8).

optimum for either CO_2 or H_2 only are shown as empty symbols.

The graphs show a trade-off between the energy consumption and the productivity for all cycles. This is related to the change in evacuation pressure along the Pareto front, as shown in Figure 10: The evacuation pressure decreases for all cycles when moving from minimum to maximum energy consumption (or minimum to maximum productivity). When decreasing the evacuation pressure, the CO_2 cyclic capacity increases, thus leading to a more efficient use of the column and allowing for longer adsorption times without the CO_2 and impurity fronts breaking through. As a result, more CO_2 is produced in a cycle, thus increasing both productivities, Pr_{CO_2} and Pr_{H_2}. The energy consumption, however, increases because the column is regenerated at lower pressures.

Moreover, it can be noted from Figures 9 and 10 that there is a significant difference between the four cycles. This indicates that both exchanging the compressor for the Rec-BD with a series of PE steps as well as the addition of a LP step play an important role in determining both energy requirement and productivity along with the optimal evacuation pressure.

4.2.1.1. Compressor versus PE. When comparing a cycle with compressor (cycle A or B) to the corresponding cycle with PE steps (cycle C or D), the configuration with the PE steps achieves always a lower minimum specific energy consumption: Cycle C has a lower minimum specific energy consumption than cycle A; cycle D has a lower minimum specific energy consumption than cycle B. This is related to the additional energy required for recompressing the Rec-BD stream in cycles A and B. Notably, cycle C also shows higher productivities compared to those of cycle A; and cycle D shows higher productivities compared to those of cycle B. This is due to the shorter duration of the PE steps in comparison to the Rec-BD and Rec-Pr step. The differences in productivity are small compared to the differences in energy consumption and do not account for scheduling constraints, as is necessary to compare cycle times in a meaningful way (see the following section).

4.2.1.2. LP Step. When comparing a cycle without LP (cycle A or C) to the corresponding cycle with LP (cycle B or D), Figure 9 shows that the addition of the LP step reduces the minimum energy consumption. This is because cycles B and D with LP achieve the required separation performance at a higher evacuation pressure, whereas cycles A and C without LP require a lower evacuation pressure to reach the minimum target CO_2 recovery of 90%, as shown in Figure 10. Therefore, the minimum energy consumption is lower for cycles with a LP step. The penalization of low evacuation pressure, as in real vacuum pumps, makes this difference even more pronounced. Besides the lower energy consumption, the maximum productivity is also higher for cycles with LP (cycle B or D) than that for the corresponding cycles without LP (cycle A or C), because of the combined effect of lowering the evacuation pressure and of purging the remaining CO_2 and impurities out of the column. It is important to note that the Pareto fronts for the cycles with LP (cycle B or D) have to be at least as good as those for the corresponding cycles without LP (cycle A or C), because cycles B and D reduce to cycles A and C when the duration of the LP approaches zero.

A better understanding of the energy consumption can be gained by analyzing the individual contributions for all four cycles. As an interesting example, the Pareto point with minimum CO_2 specific energy consumption is considered. The individual contributions along the Pareto front are provided in the Supporting Information.

The energy required for the recycle compressor in cycles A and B makes up a significant share of the overall energy consumption, which depends on the pressure $P_{Rec\text{-}BD}$, accounting for approximately a fourth (cycle A) and over a half (cycle B) of the total energy requirement. Nevertheless, for cycle A the minimum energy consumption is only slightly larger than that for cycle C without a recycle compressor, as shown in Figure 9. This is because cycle C has worse separation performance than cycle A and therefore requires a lower evacuation pressure, i.e., larger vacuum pump consumption as shown in Figure 10. For both, the final evacuation pressure is significantly below 0.1 bar, 0.025 bar for cycle C and 0.032 bar for cycle A, thereby reaching the limit of technically feasible pressures for industrial applications. However, when the LP step is included, the energy requirement for evacuation drops drastically; it reduces by more than half for cycle B compared to cycle A and by approximately two-thirds for cycle D compared to cycle C. This is due to the better separation performance achieved when adding a LP step, which translates into a higher final evacuation pressure close to 0.1 bar for both cycles C and D, as shown in Figure 10.

In terms of minimizing the energy consumption, cycle D therefore is particularly promising (as evident in Figure 9) because it combines the positive effect of adding a LP step and of replacing the compressor with a series of PE steps. It should be noted that for all the optimal points HP is carried out at ambient pressure.

4.2.2. Effect of Scheduling. So far, we have only shown the ideal productivity, i.e., the productivity for the case of zero idle times. Adsorption processes are usually accommodated in a train that consists of several columns. The same cycle is repeated in every column shifted in time. Scheduling constraints, e.g., deriving from the need of having continuous operation, lead to idle times depending on the actual number of columns. The constraints considered here are (i) a continuous feed for all cycles and (ii) a synchronization of the PE steps for cycles C and D. This requires a product storage tank for hydrogen, a buffer tank for the Rec-BD outflow, and a buffer tank for the CO_2-rich recycle stream. These constraints lead to a minimum number of columns needed to accommodate each specific cycle configuration and

DOI: 10.1021/acs.iecr.9b02817
Ind. Eng. Chem. Res. 2019, 58, 17489−17506

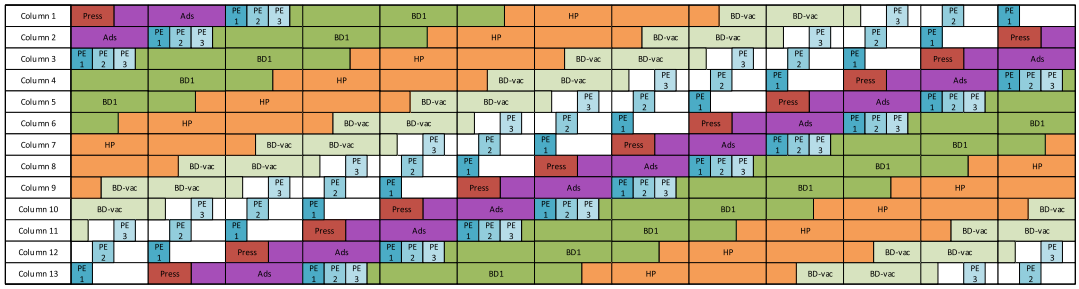

Figure 12. Schedule for cycle C for the minimum CO_2-specific energy consumption and a favorable configuration with a high effective productivity using 13 columns.

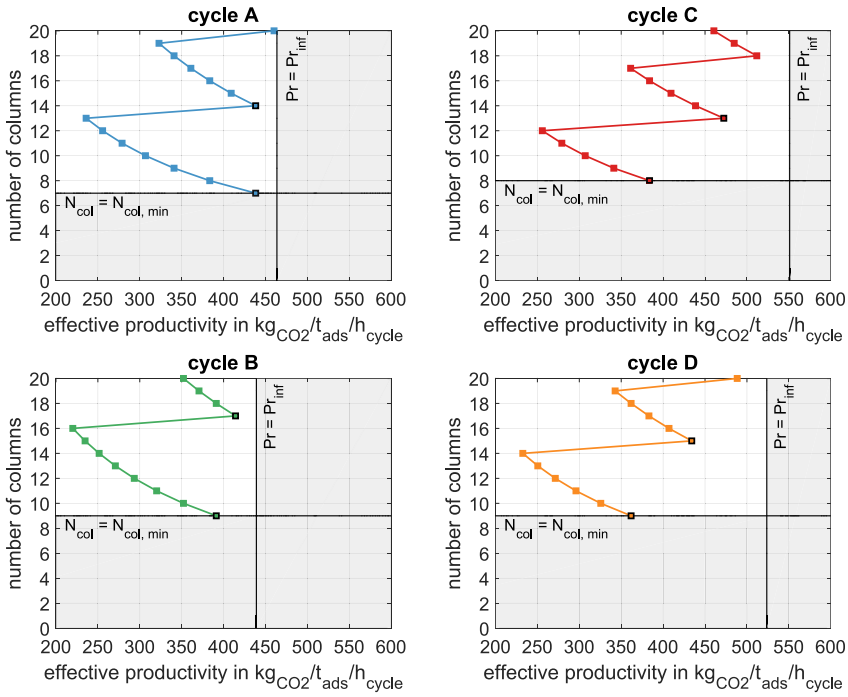

Figure 13. Effective productivity for all cycles depending on the number of columns for the Pareto point with the minimum CO_2-specific energy consumption. The maximum productivity for an infinite number of columns and zero idle times is indicated as vertical line for all cycles; the minimum number of columns is indicated as horizontal line for all cycles.

a reduced productivity compared to the ideal productivity. To enable a fair comparison of the productivities for the different cycles, the effect of scheduling therefore has to be taken into consideration.

In Figures 11 and 12, two schedules for cycle C for the point with the minimum CO_2 specific energy consumption are shown. A minimum of 8 columns is needed to accommodate the cycle and feed continuously, as shown in Figure 11. Because of the constraint of a continuous feed, the duration of the feed-receiving steps (Ads and Press) is equal to the time shift between two columns. At all times, exactly one column receives the feed. Because of the required synchronization of the PE steps, there are large idle times after PE-Pr1, PE-Pr2, and PE-Pr3.

When increasing the number of columns, the time shift between two columns stays the same to fulfill the constraint of a continuous feed. Therefore, the scheduling remains the same and an additional column will simply be idle for the duration of the time shift between two columns. When further increasing the number of columns, eventually the point is reached where the feed can be split equally between two columns, which is shown in Figure 12. This now reduces significantly the idle time because of the shorter time shift between two columns and therefore between two PE-Pr steps. It should be noted that when the feed is split equally between two or more columns continuous hydrogen production is achieved in addition to a continuous feed, as can be seen in Figure 12: The duration of the adsorption step is longer than the duration of the time shift between two columns. When adding more columns, the effective productivity will decrease until the number of columns is high enough to allow the feed to be split equally between 3 columns (or 4 or 5 or more).

The trend described for cycle C (minimum number of columns required to accommodate the cycle, decrease in productivity when increasing the number of columns until the next favorable configuration is reached, and continuous hydrogen production starting from this next favorable configuration) is similar to that for the other cycles. This is shown in Figure 13. The figure shows the effect of the number of columns on the productivity Pr_{eff} for all cycles, calculated as representative exemplary case for the Pareto point with the minimum CO_2 specific energy consumption (as shown in Figure 9a). In addition to the effective productivities, the productivity for an infinite number of columns Pr_{inf} is indicated

DOI: 10.1021/acs.iecr.9b02817
Ind. Eng. Chem. Res. 2019, 58, 17489−17506

as a vertical line, and the minimum number of columns is shown as a horizontal line.

The figure shows that there is a different minimum number of columns needed to accommodate each cycle. The minimum number of columns increases when adding the LP step to cycles A or C, because of an overall longer duration of the cycle. It is shown clearly in the figure that increasing the number of columns does not lead to a monotonic increase in productivity, but rather that the productivity is maximized for only certain numbers of columns. Departing from there, it decreases when increasing the number of columns until a new favorable configuration is reached that leads to a higher effective productivity. Once the number of columns is high enough for the feed to be split between two columns, continuous hydrogen production is achieved in addition to a continuous feed, as illustrated for cycle C above. The effective productivities for the additional constraint of a continuous hydrogen product withdrawal are the same as for a continuous feed but starting from a higher minimum number of columns. This is summarized in Table 4.

Table 4. Minimum Number of Columns Needed for Continuous Feed and Continuous H_2 Production for All Cycles[a]

	continuous feed			continuous H_2 production			zero idle times
	Pr_{CO_2} (kg_{CO_2}/(t_{ads} h))	N_{Col}	ΔPr (%)	Pr_{CO_2} (kg_{CO_2}/(t_{ads} h))	N_{Col}	ΔPr (%)	Pr_{CO_2} (kg_{CO_2}/(t_{ads} h))
cycle A	438	7	5	438	14	5	463
cycle B	391	9	11	414	17	6	439
cycle C	384	8	30	472	13	14	551
cycle D	362	9	31	434	15	17	23

[a]With the effective productivities, the ideal productivities in case of zero idle times, and the decrease in % compared to the ideal productivities, given for the point with the minimum CO_2 specific energy consumption; points shown with black outline in Figure 13.

When comparing the effective productivity with the scheduling Pr_{eff} and the ideal productivity Pr_{inf} for zero idle time for all cycles, it can be seen from Figure 13 and Table 4, that the drop in productivity is significantly lower for cycles A and B than that for cycles C and D. This is due to the additional constraint of synchronizing the PE steps in cycles C and D. This constraint leads to large idle times, i.e., in the range of 3 times the time shift between two columns, whereas for cycles A and B, the idle time is shorter, i.e., in the range of the time shift between two columns. As a consequence, when using the minimum number of columns, the effective productivities of cycles C and D drop below those of cycles A and B, respectively. This is in contrast to the ideal productivities with zero idle time that are larger for cycles C and D than for cycles A and B. For cycles C and D, the gain when increasing the number of columns to the next higher favorable configuration, e.g., 13 columns instead of 8 columns for cycle C, is high (>22% increase in productivity), whereas for cycles A and B, there is almost no improvement in productivity.

4.3. Overall Cycle Assessment. All four cycles presented above can co-produce hydrogen and CO_2 at 90% recovery and 95% purity for both products. Cycle B (with LP), however, outperforms cycle A (without LP) in all respects (better CO_2 separation performance, better hydrogen separation performance, lower specific energy consumption, and higher effective productivity for the same energy consumption and number of columns), and cycle D (with LP) outperforms cycle C (without LP) in all respects. Therefore, only cycles B and D will be considered further.

The Pareto curves for minimizing the CO_2 specific energy consumption and maximizing the productivity for purities ≥95% and recoveries ≥90% for both products are shown in Figure 12 for an infinite number of columns (empty symbols) and for the minimum number of columns required when accounting for the scheduling (filled symbols). The minimum number of columns required decreases with increasing productivities. This is due to an increase in the duration of the adsorption step.

Figure 14 shows that cycle D is clearly superior in terms of the minimum energy consumption. Because of the LP step,

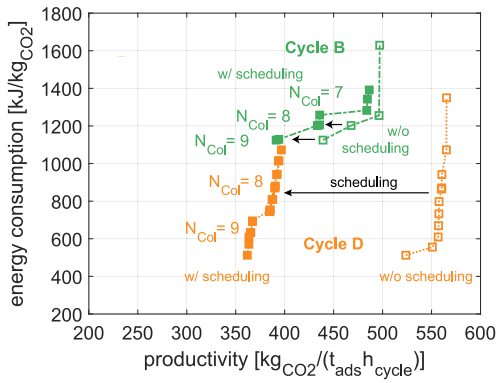

Figure 14. CO_2 specific energy consumption and productivity for cycles B and D with scheduling (filled symbols) and ideal productivity Pr_{inf} for an infinite number of columns (empty symbols); effective productivity calculated for the minimum number of columns as indicated. Constraints: $r_{H_2} \geq 90\%$, $\Phi_{H_2} \geq 95\%$, $r_{CO_2} \geq 90\%$, $\Phi_{CO_2} \geq 95\%$.

cycle D achieves the separation with a relatively high evacuation pressure (in contrast to cycles A and C) and without the need of a compressor for recycling the hydrogen-rich Rec-BD outflow as PE are used instead (in contrast to cycles A and B). The maximum effective productivity for cycle D, however, is lower than that for cycle B due to the additional constraint of synchronizing the PE steps when scheduling cycle D.

In addition to the higher effective productivity and the lower minimum number of columns for the target separation, cycle B is particularly promising when higher hydrogen purities and/or recoveries are needed. This is due to more precise control over the pressure, until which the hydrogen-rich outflow after the adsorption step is recycled. The pressure at the end of three PE steps is in the range of 4−5 bar, which is favorable for reaching the target CO_2 separation performance. For maximum Φ_{H_2} and targeted r_{H_2} = 90%, however, a lower pressure of around 3 bar is favorable; for maximizing r_{H_2} for Φ_{H_2} = 95%, an even lower pressure of just above 1 bar is required. Notably, neither is reached with three PE steps. An option for maximizing either hydrogen purity or recovery while still fulfilling the three other constraints would be the addition of more PE steps to cycle D. This, however, would result in a more complicated schedule with an increase in the minimum number of columns and a

DOI: 10.1021/acs.iecr.9b02817
Ind. Eng. Chem. Res. 2019, 58, 17489−17506

further decrease in Pr_{eff}. In addition, a cycle with PE steps will never cover the whole range of hydrogen recoveries and purities, as it is possible with cycle B.

Thus, summarizing, when considering all factors, namely, the separation requirements, the flexibility requirements, the cost of adsorbent, columns, and compressor, the use of the hydrogen product, and the price of electricity, either cycle B or D might be the best choice.

4.4. Comparison of Cycle Performance to the State-of-the-Art Technology. To put the performance of the developed VPSA cycles into perspective, a comparison with the absorption-based CO_2 capture process is needed. To this end, we first need to have a fair energy comparison: Whereas the VPSA process requires electricity for evacuation and compression, the energy required for absorption-based processes is a combination of heat (in the form of low-pressure steam for regenerating the CO_2-rich solution) and electricity (required for pumps, chilling, and recycle compressors). To account for the different forms of the required energy, we have computed the overall exergy e_x for both processes. While for the VPSA, the exergy consumption corresponds to the electricity consumption, i.e., electricity is pure exergy; for the reference, we need to convert the heat requirement into exergy. Accordingly, the reboiler heat duty for solvent regeneration is converted to exergy by means of the Carnot factor, which is computed between the reboiler temperature $T_{Reboiler}$ and ambient temperature T_{amb}, here taken as 298 K. The resulting exergy consumption of the state-of-the-art process is as follows:

$$e_x = e_{Reboiler}\left(1 - \frac{T_{amb}}{T_{Reboiler}}\right) + e_{el} \tag{6}$$

Concerning the productivity of the state-of-the-art process, different values are available in the literature, most notably, the detailed design of Shell Quest project (via Alberta's CCS Knowledge Sharing Program).[4,27−29] Here, for simplicity we calculate the productivity of the reference by only considering the CO_2 absorber and desorber.

The process performance of the VPSA in comparison to absorption-based CO_2 capture is illustrated in Figure 15. The productivity is given per equipment volume and has been calculated for the adsorption processes with the bed density as reported in Table 1.

The energy required when using MDEA depends on the target capture rate and can be reduced with advanced flowsheet configurations. The typical exergy consumption is in the range of 300−600 kJ/kg_{CO_2}, including the thermal energy required for the reboiler and the electricity consumption for the pumps, with productivities below 100 kg_{CO_2}/(m^3 h).[4,28−30] The energy required when using physical solvents, which typically feature higher syngas pressure and/or higher concentration of CO_2 in the feed, is around 200−400 kJ/kg_{CO_2}.[31]

When comparing absorption-based capture processes with the developed VPSA cycles, the figure shows that only cycle D can reach the upper range of the reported energy consumptions for MDEA, whereas the energy consumption for cycle B is significantly higher. However, the productivity for both cycles is higher than the values reported for MDEA. In addition, the use of electricity instead of steam reduces the process complexity significantly. Therefore, in our opinion cycle D presents a promising alternative to absorption-based CO_2 capture.

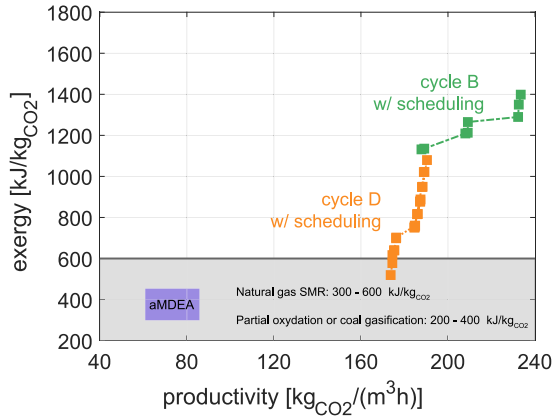

Figure 15. Comparison of the process performance for VPSA cycles B and D with scheduling, and absorption-based carbon capture, including physical and chemical solvents. The energy consumption for state-of-the-art processes depends on the syngas production route, and is typically in the range of 300−600 kJ/kg_{CO_2} for natural gas SMR, e.g., with MDEA, and 200−400 kJ/kg_{CO_2} for partial oxidation or coal gasification, e.g., with Selexol, Purisol, or Rectisol. A more specific area is highlighted for aMDEA, the state-of-the-art technology for SMR processes, using the following references: (i) Shell QUEST project via the Alberta's CCS Knowledge Sharing Program:[27] e_x = 414 kJ/kg_{CO_2} without heat integration, e_x = 325 kJ/kg_{CO_2} with heat integration, and Pr_{eff} = 71 kg_{CO_2}/m^3/h. (ii) IEAGHG reports on hydrogen production:[4,28] e_x = 318 kJ/kg_{CO_2} and Pr_{eff} = 86 kg_{CO_2}/m^3/h. (iii) Romano et al.:[29] e_x = 317 kJ/kg_{CO_2}. For the exergy calculation, the reboiler duty has been multiplied with the Carnot factor using the reboiler steam temperature, which is provided in the references. For the productivity, only absorbers and stripper have been considered. Constraints for VPSA: $r_{H_2} \geq 90\%$, $\Phi_{H_2} \geq 95\%$, $r_{CO_2} \geq 90\%$, $\Phi_{CO_2} \geq 95\%$.

In addition to separating CO_2, VPSA also purifies hydrogen up to high purities, thereby combining two separation tasks in one unit. When using absorption-based CO_2 capture systems, an additional PSA unit after absorption is required for hydrogen purification (compare Figure 1). Because the inlet stream is already available at high pressure, no additional energy is required for the PSA.

By eliminating a whole separation stage while having a separation performance similar to that of the reference system (MDEA capture + PSA), VPSA cycle D allows for (i) a reduction in complexity and (ii) an increase in productivity compared to the state-of-the-art technology while featuring an energy consumption comparable to the upper end of values reported for MDEA capture. Both features might lead to a significant reduction in capital cost compared to MDEA + PSA.

5. CONCLUSION

In this article, we have presented the development and assessment of new adsorption cycles for co-production of CO_2 and H_2 from a ternary feed with significant amount of impurity. Four different VPSA cycles have been developed and optimized. The main differences between the cycles are (i) how the hydrogen-rich outflow is recycled, either via a compressor or a sequence of pressure equalization (PE)

DOI: 10.1021/acs.iecr.9b02817
Ind. Eng. Chem. Res. 2019, 58, 17489−17506

steps, and (ii) how the bed is purged after the CO_2 step, i.e., introducing a hydrogen light purge (LP) step or not. While the LP step is favorable for the CO_2 separation performance, using a compressor increases the H_2 separation performance.

For very high purities of both products, a cycle with compressor and LP step is therefore the most promising, namely, cycle B.

For the targeted co-production of high-purity H_2 and CO_2 (minimum 95% purity) with high recoveries for both products (minimum 90% recovery), however, PE steps are sufficient. When including the evacuation pressure in the optimization, all cycles can achieve this separation target. Adding a LP step, however, decreases the energy consumption significantly because the separation can be achieved at higher evacuation pressures. In addition, exchanging the compressor with PE steps reduces the energy consumption even further. Therefore, for the given separation target, a cycle with PE steps and a LP is the most promising option to minimize the energy consumption, namely cycle D.

When scheduling into a continuous process, the different cycles require a minimum of 7−9 columns and have a similar productivity.

Comparing the VPSA cycles to state-of-the-art CO_2 capture processes in hydrogen production plants (considering also public data of existing processes) reveals two interesting aspects. First, the volumetric productivity of the presented VPSA cycles is 2-fold that of the state-of-the-art process. Second, the exergy consumption of cycle D is within the range of reported absorption processes. Whereas the state-of-the-art process adopts two separation stages, one for CO_2 capture and another one for H_2 purification, the VPSA cycles integrate hydrogen purification and CO_2 separation within a single separation process, which makes them promising for process intensification. Overall, cycle D is especially interesting for further development due to the competitive exergy consumption in addition to the high productivity. Tangible options exist to further improve its performance.

In an effort to keep our results general, we used a commercial AC as sorbent, but we do not expect it to be the optimal choice. Layering of different sorbents or the use of novel sorbent materials, e.g., metal−organic-frameworks, with a higher cyclic capacity for CO_2 is expected to further reduce exergy consumption while also increasing productivity.

Whereas a very generic inlet stream with N_2 as impurity has been chosen for cycle design and development, the cycles proposed here are promising also for separations with different feed stream compositions, as long as H_2 and CO_2 are the light and heavy component, respectively. This includes feed streams with CH_4 or CO as main impurity or a mixture of different impurities, i.e., N_2, CH_4, and CO. With reference to the application of this technology to SMR, which is beyond the scope of this manuscript and will be discussed in a dedicated follow up paper, our preliminary results indicate that cycle D can successfully purify hydrogen up to greater 99.99% purity at around 90% recovery while also separating CO_2 with CCS specifications at an exergy penalty below 600 kJ/kg_{CO_2}. With the choice of an appropriate adsorbent or with a layering of different adsorbent materials, these cycles could therefore enable a variety of separations relevant for hydrogen production coupled with CCS.

■ ASSOCIATED CONTENT

Supporting Information

The Supporting Information is available free of charge on the ACS Publications website at DOI: 10.1021/acs.iecr.9b02817.

- Model equations: mass, energy and momentum balance equations, EOS, correlation for mass transfer, isotherm parameters, calculation of the energy consumption for evacuating the column, scheduling equations, study of influence of decision variables on separation performance, internal column profiles for representative simulations of cycles A and B, and contribution of vacuum pump and compressor to the total energy consumption (PDF)

■ AUTHOR INFORMATION

Corresponding Authors

*E-mail: m.gazzani@uu.nl (M.G.).

*E-mail: marco.mazzotti@ipe.mavt.ethz.ch (M.M.).

ORCID

Anne Streb: 0000-0001-8159-707X

Matteo Gazzani: 0000-0002-1352-4562

Marco Mazzotti: 0000-0002-4948-6705

Notes

The authors declare no competing financial interest.

■ ACKNOWLEDGMENTS

We thank Dr. Lisa Joss (School of Chemical Engineering & Analytical Science, The University of Manchester) for the many fruitful discussions during the preliminary phase of this work. ACT ELEGANCY, Project No 271498, has received funding from DETEC (CH), BMWi (DE), RVO (NL), Gassnova (NO), BEIS (UK), Gassco, Equinor and Total, and is cofunded by the European Commission under the Horizon 2020 programme, ACT Grant Agreement No 691712. This project is supported by the pilot and demonstration programme of the Swiss Federal Office of Energy (SFOE).

■ ABBREVIATIONS

Acronyms

AC	activated carbon
Ads	adsorption step
BD1	blowdown to heavy purge
BD-vac	pressure blowdown to subatmospheric pressure
C	compressor
CCS	carbon dioxide capture and storage
CSS	cyclic steady state
EOS	equation of state
HP	heavy purge
LP1	purge with light product (here: H_2), outflow recycled to heavy purge
LP2	purge with light product (here: H_2), outflow wasted
MDEA	methyl diethanolamine
MO-MCS	multiobjective multilevel coordinate search
MCS	multilevel coordinate search
PE	pressure equalization
PE-BD	pressure equalization - blowdown
PE-Pr	pressure equalization - pressurization
Press	pressurization, here: with feed
PSA	pressure swing adsorption
Rec-BD	recycling blowdown step

DOI: 10.1021/acs.iecr.9b02817
Ind. Eng. Chem. Res. 2019, 58, 17489−17506

Rec-Pr	pressurization with recycle, here: H_2-rich stream
SMR	steam methane reforming
VP	vacuum pump
VPSA	vacuum pressure swing adsorption
VSA	vacuum swing adsorption

Symbols

C_s	heat capacity of adsorbent [J/kg/K]
d_i	internal column diameter [m]
d_P	particle diameter [m]
$\Delta H_{Ads,i}$	isosteric heat of adsorption [J/mol]
e	specific energy consumption [kJ/kg$_{Product}$]; eq 4,
$e_{Reboiler}$	CO_2 specific reboiler heat duty [kJ/kg$_{CO_2}$]
e_{el}	CO_2 specific electricity consumption [kJ/kg$_{CO_2}$]
e_x	CO_2 specific exergy consumption [kJ/kg$_{CO_2}$]; eq 6
E_{HP}	energy required to compress the recycled part of the CO_2 product from ambient pressure to P_{HP} (in case the HP is carried out above ambient pressure) [kJ]
E_{H_2}	energy required for recompressing the hydrogen-rich stream [kJ]
E_{tot}	total energy consumption [kJ]
E_{VP}	energy required for evacuating the column and purging under vacuum [kJ]
i	component [-]
k_i	mass transfer coefficient, linear driving force approximation [1/s]
L_{col}	column length [m]
$M_{W,i}$	molecular weight of component i [kg/mol]
N_{col}	number of columns [-]
$N_{col,min}$	minimum number of columns [-]
$N_{i,Prod}$	molar amount of component i in the product rich in i [mol]
$N_{tot,Prod}$	molar amount of product rich in i [mol]
$N_{i,tot}$	total molar amount of component i fed to one cycle [mol]
P_{Ads}	column pressure at the end of Press and during Ads [bar]
P_{Amb}	ambient pressure [bar]
$P_{BD\text{-}vac}$	column pressure at the end of BD-vac [bar]
P_{Feed}	feedstream pressure [bar]
P_{HP}	column pressure at the end of BD1 and during HP [bar]
$P_{Rec\text{-}BD}$	column pressure at the end of Rec-BD [bar]
P_s	column pressure of step s [bar]
P_{low}	lowest column pressure reached at the end of infinitely long BD or BD-vac step [bar]; eq 1
P_{high}	column pressure at the beginning of BD or BD-vac step [bar]; eq 1
Pr_{inf}	ideal productivity for an infinite number of columns [kg$_{CO_2}$/(t$_{ads}$h$_{cycle}$)]
Pr_{eff}	effective productivity [kg$_{CO_2}$/(t$_{ads}$h$_{cycle}$)]; eq 5; for comparison with state-of-the-art process as volumetric productivity [kg$_{CO_2}$/m^3/h]
r_i	recovery of component i [-]; eq 3
rr	recycle ratio: ratio between the recycled to the total molar outflow of a specific step [-]
s	specific step in an adsorption cycle, i.e., Ads, Press, i.a. [-]
t_{Ads}	duration of Ads [s]
$t_{Ads,LP1/2}$	duration of Ads, during which all outflow is used to purge the column [s]
$t_{BD\text{-}vac}$	duration of BD-vac [s]
t_{cycle}	cycle duration not including idle times [s]
t_{idle}	duration of idle times [s]
$t_{LP1/2}$	duration of LP1/LP2 [s]
t_s	duration of step s [s]
T_{amb}	ambient temperature, here: 298 K
T_{Feed}	feed temperature [K]
$T_{Reboiler}$	reboiler temperature [K]
V_{col}	column volume [m$_3$]
$\dot{V}_{Feed}$	feed volumetric flowrate [m^3/s]
$\mathbf{x}$	decision variables vector
$y_{i,Feed}$	molar fraction of component i in feed [mol/mol]
η_{is}	isentropic efficiency [-]
Φ_i	purity of product rich in component i [-], eq 2
ρ_b	bulk density [kg/m^3]
ρ_M	density of adsorbent material [kg/m^3]
ρ_P	density of adsorbent particles [kg/m^3]
ξ	fitting parameter describing the pressure decrease at the column outlet during blowdown and evacuation [-]; eq 1

REFERENCES

(1) Masson-Delmotte, V., Zhai, P., Pörtner, H.-O., Roberts, D., Skea, J., Shukla, P. R., Pirani, A., Moufouma-Okia, W., Péan, C., Pidcock, R., Connors, S., Matthews, J. B. R., Chen, Y., Zhou, X., Gomis, M. I., Lonnoy, E., Maycock, T., Tignor, M., Waterfield, T., Eds. *Special Report: Global warming of 1.5° C*; IPCC, 2018.

(2) Sircar, S.; Golden, T. C. Purication of Hydrogen by Pressure Swing Adsorption. *Sep. Sci. Technol.* **2000**, *35*, 667−687.

(3) Bui, M.; et al. Carbon capture and storage (CCS): the way forward. *Energy Environ. Sci.* **2018**, *11*, 1062−1176.

(4) *Techno - Economic Evaluation of SMR Based Standalone (Merchant) Hydrogen Plant with CCS*; IEAGHG, 2017.

(5) Sircar, S.; Kratz, W. C. Simultaneous Production of Hydrogen and Carbon Dioxide from Steam Reformer Off-Gas by Pressure Swing Adsorption. *Sep. Sci. Technol.* **1988**, *23*, 2397−2415.

(6) Baade, W. F.; Farnand, S.; Hutchison, R.; Welch, K. CO_2 capture from SMRs: A demonstration project. *Hydrocarbon Processing* **2012**, *91*, 63−68.

(7) Palamara, J.; Guvelioglu, G.; Carney, S. Air products: success in advanced separation and CO_2 processing for EOR. *19th Annual CO_2 Flooding Conference*, December 12, 2013.

(8) *Carbon Capture Technology Program Plan*; U.S. Department of Energy, Clean Coal Research Program, 2013.

(9) *Quality Guidelines for Energy System Studies: CO_2 Impurity Design Parameter*; DOE/NETL-341/011212, Rev 3 ; NETL, 2013.

(10) de Visser, E.; Hendriks, C.; Barrio, M.; Mølnvik, M. J.; de Koeijer, G.; Liljemark, S.; Le Gallo, Y. Dynamis CO_2 quality recommendations. *Int. J. Greenhouse Gas Control* **2008**, *2*, 478−484.

(11) Streb, A.; Hefti, M.; Gazzani, M.; Mazzotti, M. A pressure swing adsorption process. EP191723840.0, 2019.

(12) Schell, J.; Casas, N.; Marx, D.; Mazzotti, M. Precombustion CO_2 Capture by Pressure Swing Adsorption (PSA): Comparison of Laboratory PSA Experiments and Simulations. *Ind. Eng. Chem. Res.* **2013**, *52*, 8311−8322.

(13) Marx, D.; Joss, L.; Hefti, M.; Gazzani, M.; Mazzotti, M. CO_2 Capture from a Binary CO_2/N_2 and a Ternary $CO_2/N_2/H_2$Mixture by PSA: Experiments and Predictions. *Ind. Eng. Chem. Res.* **2015**, *54*, 6035−6045.

(14) Marx, D.; Joss, L.; Hefti, M.; Mazzotti, M. Temperature Swing Adsorption for Post-combustion CO_2 Capture: Single- and Multi-column Experiments and Simulations. *Ind. Eng. Chem. Res.* **2016**, *55*, 1401−1412.

(15) Joss, L.; Gazzani, M.; Mazzotti, M. Rational design of temperature swing adsorption cycles for post-combustion CO_2 capture. *Chem. Eng. Sci.* **2017**, *158*, 381−394.

DOI: 10.1021/acs.iecr.9b02817
Ind. Eng. Chem. Res. 2019, 58, 17489−17506

(16) Hefti, M.; Mazzotti, M. Postcombustion CO_2 Capture from Wet Flue Gas by Temperature Swing Adsorption. *Ind. Eng. Chem. Res.* **2018**, *57*, 15542−15555.
(17) Casas, N.; Schell, J.; Pini, R.; Mazzotti, M. Fixed bed adsorption of CO_2/H_2 mixtures on activated carbon: experiments and modeling. *Adsorption* **2012**, *18*, 143−161.
(18) Casas, N.; Schell, J.; Joss, L.; Mazzotti, M. A parametric study of a PSA process for pre-combustion CO_2 capture. *Sep. Purif. Technol.* **2013**, *104*, 183−192.
(19) Marx, D.; Joss, L.; Casas, N.; Schell, J.; Mazzotti, M. Prediction of non-isothermal ternary gas-phase breakthrough experiments based on binary data. *Adsorption* **2014**, *20*, 493−510.
(20) Schell, J.; Casas, N.; Pini, R.; Mazzotti, M. Pure and binary adsorption of CO_2, H_2, and N_2 on activated carbon. *Adsorption* **2012**, *18*, 49−65.
(21) Hefti, M.; Marx, D.; Joss, L.; Mazzotti, M. Adsorption equilibrium of binary mixtures of carbon dioxide and nitrogen on zeolites ZSM-5 and 13X. *Microporous Mesoporous Mater.* **2015**, *215*, 215−228.
(22) Hefti, M.; Mazzotti, M. Modeling water vapor adsorption/desorption cycles. *Adsorption* **2014**, *20*, 359−371.
(23) Li, G.; Xiao, P.; Zhang, J.; Webley, P. A.; Xu, D. The role of water on postcombustion CO_2 capture by vacuum swing adsorption: Bed layering and purge to feed ratio. *AIChE J.* **2014**, *60*, 673−689.
(24) Krishnamurthy, S.; Haghpanah, R.; Rajendran, A.; Farooq, S. Simulation and Optimization of a Dual-Adsorbent, Two-Bed Vacuum Swing Adsorption Process for CO_2 Capture from Wet Flue Gas. *Ind. Eng. Chem. Res.* **2014**, *53*, 14462−14473.
(25) Krishnamurthy, S.; Rao, V. R.; Guntuka, S.; Sharratt, P.; Haghpanah, R.; Rajendran, A.; Amanullah, M.; Karimi, I. A.; Farooq, S. CO_2 capture from dry flue gas by vacuum swing adsorption: A pilot plant study. *AIChE J.* **2014**, *60*, 1830−1842.
(26) Capra, F.; Gazzani, M.; Joss, L.; Mazzotti, M.; Martelli, E. MO-MCS, a Derivative-Free Algorithm for the Multiobjective Optimization of Adsorption Processes. *Ind. Eng. Chem. Res.* **2018**, *57*, 9977−9993.
(27) Alberta's CCS Knowledge Sharing Program. https://open.alberta.ca/dataset?tags=CCS+knowledge+sharing+program&=Quest+Carbon+Capture+and+Storage+project (accessed March 04, 2019).
(28) *Techno-Economic Evaluation of HYCO Plant Integrated to Ammonia/Urea or Methanol Production with CCS*; Report No. 2017-03; IEAGHG, 2017.
(29) Romano, M. C.; Chiesa, P.; Lozza, G. Pre-combustion CO_2 capture from natural gas power plants, with ATR and MDEA processes. *Int. J. Greenhouse Gas Control* **2010**, *4*, 785−797.
(30) Meissner, R. I.; Wagner, U. Low-energy process recovers CO_2. *Oil Gas J.* **1983**, *81*, 55−58.
(31) Burr, B. L.; Lyddon, L. A comparison of physical solvents for acid gas removal. In *87th Annual GPA Convention*, 2008.

DOI: 10.1021/acs.iecr.9b02817
Ind. Eng. Chem. Res. 2019, 58, 17489−17506